Frequency Control of DFIG based Wind Power Penetrated Power Systems Using Switching Angle Controller and AGC

Y. Liu, L. Jiang, *Member, IEEE*, Q. H. Wu, *Fellow, IEEE*, X. X. Zhou, *Fellow, IEEE*

***Abstract*—This paper proposes a switching angle controller (SAC) and an automatic generation controller (AGC) for the doubly-fed induction generator (DFIG) to control the frequency of DFIG-based wind power penetrated power systems (WPPSs). The concept of virtual rotor angle of the DFIG is defined. The virtual rotor angle is controlled by the SAC in a bang-bang manner such that the active power of the DFIG is regulated to provide frequency support to the external power grids. The output of the SAC is also used for the control of pitch angle to offer a short-term regulation of the mechanical power input to the DFIG, and the long-term control of the mechanical power input is achieved with the AGC. Small-signal analysis is undertaken to verify the effectiveness of the SAC and the AGC. Simulation studies are carried out in a two-machine power system and a modified Kundur four-machine two-area power system, respectively. The frequency support performance of DFIGs having different control configurations is investigated. Modal analysis is undertaken to evaluate the effect of the SAC and the AGC in providing additional damping to the rotor oscillation modes of the modified Kundur four-machine two-area power system.**

***Index Terms*—AGC, DFIG, frequency control, switching angle controller, virtual rotor angle.**

I. Introduction

The variable speed wind power generation systems, such as the DFIG-based wind turbines, are widely used in industry for their relatively high efficiency and low cost [1]. Due to the power electronic interfaces and the accurate phase tracking performance of the phase-locked loop (PLL) [2], [3], the variable speed wind power generation systems are immune to system frequency excursions, which can weaken the frequency stability of conventional power systems as the share of wind power generation increases [4]. To solve this problem, two kinds of control strategies are utilized in wind power generators (WPGs) to control the frequency of WPPSs.

This work was funded in part by the State Key Program of National Science of China (No. 51437006), Guangdong Innovative Research Team Program (No. 201001N0104744201), National Natural Science Foundation of China (No. 51428702), China, and Engineering and Physical Sciences Research Council (No. EP/J014249/1), UK.

Y. Liu and Q. H. Wu are with the School of Electric Power Engineering, South China University of Technology, Guangzhou, 510640, China (Corresponding author: Q. H. Wu, e-mail: wuqh@scut.edu.cn), and they are also with the Department of Electrical Engineering and Electronics, The University of Liverpool, Liverpool, L69 3GJ, U.K.

L. Jiang is with the Department of Electrical Engineering and Electronics, The University of Liverpool, Liverpool, L69 3GJ, U.K.

X. X. Zhou is with China Electric Power Research Institute, State Grid Corporation of China, Qinghe, Beijing, 100192, China.

The first group of control methods enable WPGs to take part in the primary frequency control by the de-loading operation of WPGs [5]. Namely, the active power output of WPGs is reserved instead of tracking the maximum power point. Hence, they can ramp their active power outputs up and down in the frequency excursion events to provide frequency support to the external power grids. To realize the de-loading operation of WPGs, over-speeding techniques and pitching techniques were introduced. The over-speeding techniques de-load a WPG by accelerating its rotor to a speed value greater than its maximum power tracking value [6]. An example was presented in [7], in which a de-loaded power versus rotor speed lookup table was used for the de-loading operation of DFIGs. Similar scheme was proposed in [8]. Nevertheless, the over-speeding techniques are only preferable in the cases where WPGs operate below rated wind speed conditions [5]. With respect to the pitching techniques, they de-load WPGs though increasing their pitch angle such that the active power outputs are reserved and specific power margin is obtained. The examples of this approach can be found in [9], [10], in which it manifested that primary frequency support of WPGs can be attained by pitch angle control.

The second group of control strategies are referred to as virtual inertia control. By the virtual inertia control, the WPGs are controlled to emulate the behaviour of synchronous generators in frequency excursion events. For example, the torque set point of the speed control loop of a WPG was regulated with the deviation of grid frequency and its changing rate in [11]. In [12], a synchronous generator model was embedded in the rotor side controller of a WPG such that the active power output of the WPG is regulated according to a rotor motion equation. Actually, the virtual inertia control is realized on the basis of the de-loading operation of WPGs as well, because the primary frequency control requires the WPGs to increase their active power output when system frequency is lower than its nominal value. Besides the above, energy storage devices were also used for the frequency control of WPPSs in [13], [14], in which the inertial response of WPGs was achieved by the bidirectional active power control of energy storage devices. However, the disadvantage of using energy storage devices for frequency control lies in their high cost.

Based upon the de-loading operation of WPGs realized by pitch control, this paper proposes a SAC and an AGC for the DFIG to control the frequency of DFIG-based WPPSs. Compared with the existing studies [5]–[14], the SAC is a discrete controller with only two control values. It adjusts the

active power output of the DFIG by directly controlling the angle between the internal voltage and the terminal voltage of the DFIG, which is defined as the virtual rotor angle here. It enables the DFIG to response to the system frequency deviation in a bang-bang manner. The advantages of the SAC in comparison to the continuous controllers are twofold. On one hand, the fast response capability of the converter controlled active power of the DFIG is fully explored by the SAC. Then the DFIG controlled by the SAC can provide faster active power support than that controlled by the continuous controllers. On the other hand, the continuous controllers respond to frequency excursions of all magnitudes and frequencies, whilst the SAC can only be triggered when frequency deviation exceeds the pre-specific boundaries. Therefore, the SAC has stronger robustness to the small-magnitude oscillations and measurement noise of system frequency. Similar to the AGC of a synchronous generator, an AGC is embedded in the pitch angle control loop of the DFIG here. It enables the DFIG to take part in the primary and secondary frequency control of power systems.

The frequency control methods proposed here work on the basis of the de-loading operation of DFIGs [5]–[10], which is realized by the pitching technique [9], [10]. In contrast to the method proposed in [11], the SAC and the AGC do not introduce any derivative items in their control loops. The SAC and the AGC serve as complementary controllers for the conventional vector control system of DFIGs. They are easier to apply in practice than the method presented in [12], in which completely new control system was employed for the rotor-side converter (RSC) of a DFIG and another vector controller must be used for the grid-side converter (GSC). Compared with the work illustrated in [13], [14], the SAC and AGC proposed here do not add costs on WPGs. The contributions of this work can be summarized as follows.

The concept of virtual rotor angle is defined for the DFIG according to its steady-state equivalent circuit. A SAC is designed for the rapid regulation of the active power output of the DFIG by adjusting its virtual rotor angle in a bang-bang manner. The pitch angle of the DFIG is controlled by the combined effort of the SAC and an AGC. The SAC provides a short-term regulation while the AGC offers a long-term control, which ensures the coordination between the mechanical power input and the active power output of the DFIG. Moreover, the small-signal model of an entire DFIG system, which includes the aerodynamical model of a wind turbine, an induction generator, a pitch angle controller, a vector control system, and a PLL, is investigated. Furthermore, simulation studies are undertaken in a two-machine power system and a modified Kundur four-machine two-area power system, respectively. The frequency control performance of DFIGs having only the AGC, only the SAC, both the SAC and AGC, and virtual inertia controller [15] installed respectively is evaluated. Modal analysis of the modified Kundur four-machine two-area power system is carried out to evaluate the effect of the proposed controllers in providing additional damping to the rotor oscillation modes of the system.

Overall, this paper is organized as follows. The internal voltage and the virtual rotor angle of the DFIG are defined in Section II. Section III is devoted to the design of the SAC and the AGC. The small-signal analysis of the DFIG equipped with the SAC and the AGC is undertaken in Section IV. Simulation studies are carried out in Section V. Conclusions are draw in Section VI, and appendices follow thereafter.

II. Internal Voltage and Virtual Rotor Angle of DFIGs

The steady-state voltage equations of a DFIG can be denoted as follows [16].

$$\begin{cases} \overrightarrow{V}_{\rm s} = R_{\rm s}\overrightarrow{I}_{\rm s} + j\omega_{\rm s}L_{\rm ls}\overrightarrow{I}_{\rm s} + j\omega_{\rm s}L_{\rm m}(\overrightarrow{I}_{\rm s} + \overrightarrow{I}_{\rm r}) \\ \frac{\overrightarrow{V}_{\rm r}}{s} = \frac{R_{\rm r}}{s}\overrightarrow{I}_{\rm r} + j\omega_{\rm s}L_{\rm lr}\overrightarrow{I}_{\rm r} + j\omega_{\rm s}L_{\rm m}(\overrightarrow{I}_{\rm s} + \overrightarrow{I}_{\rm r}) \end{cases} \tag{1}$$

where all the symbols are explained in Appendix A. The steady-state equivalent circuit of the DFIG can be presented as shown in Fig. 1 (a), where $\overrightarrow{I}_{\rm ms}$ is the excitation current of the DFIG and defined as $\overrightarrow{I}_{\rm ms} = \overrightarrow{I}_{\rm s} + \overrightarrow{I}_{\rm r}$. Based upon the *Thevenin's theorem*, this circuit is equivalent to the one presented in Fig. 1 (b), where $R_{\rm eq} = R_{\rm s} + \frac{\omega_{\rm s}^2 L_{\rm m}^2 R_{\rm r}/s}{(R_{\rm r}/s)^2+(\omega_{\rm s}L_{\rm r})^2}$ and $L_{\rm eq} = L_{\rm ls} + \frac{L_{\rm m}[\omega_{\rm s}^2 L_{\rm lr}L_{\rm r}+(R_{\rm r}/s)^2]}{(R_{\rm r}/s)^2+(\omega_{\rm s}L_{\rm m})^2}$. Then the internal voltage of the DFIG can be denoted as

$$\overrightarrow{E}_{\rm ms} = \frac{s\omega_{\rm s}^2 L_{\rm m}L_{\rm r} + j\omega_{\rm s}L_{\rm m}R_{\rm r}}{R_{\rm r}^2 + (s\omega_{\rm s}L_{\rm r})^2}\overrightarrow{V}_{\rm r} \tag{2}$$

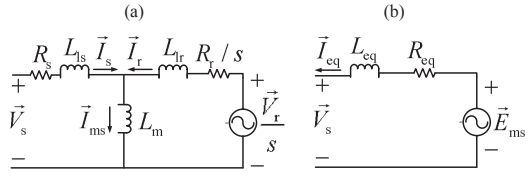

Fig. 1. Steady-state circuit of the DFIG and its equivalent circuit.

Let $\overrightarrow{V}_{\rm s} = V_{\rm s}\angle\theta_{\rm s}$, and $\overrightarrow{E}_{\rm ms} = E_{\rm ms}\angle(\theta+\theta_{\rm s})$, where θ is defined as the virtual rotor angle of the DFIG. The active power output from $\overrightarrow{E}_{\rm ms}$ to $\overrightarrow{V}_{\rm s}$ is $P_{\rm e} = \frac{V_{\rm s}}{\sqrt{R_{\rm eq}^2+X_{\rm eq}^2}}[R_{\rm eq}(E_{\rm ms}\cos\theta - V_{\rm s}) + X_{\rm eq}E_{\rm ms}\sin\theta]$. Note that $X_{\rm eq}$ is more than ten times larger than $R_{\rm eq}$ in the normal operation of a DFIG, thus the active power output of the DFIG can be simply expressed by $P_{\rm e} = \frac{E_{\rm ms}V_{\rm s}}{X_{\rm eq}}\sin\theta$. Taking the DFIG with parameters presented in Appendix C as an example, the $P_{\rm e}$ versus θ is shown in Fig. 2 (a). The speed-droop characteristics of a synchronous generator is presented in Fig. 2 (b). For frequency support to the external power grids, the active power output of the DFIG is desirable to behave like that of a synchronous generator [17]. In the cases where system frequency drops, the active power of the DFIG is desirable to increase, which can be realized by increasing θ as shown in Fig. 2 (a). Analogously, θ should be decreased in the cases where system frequency overrides its nominal value. To realize this, a SAC is designed in the following section.

III. SAC and AGC Design

The SAC controls the virtual rotor angle of the DFIG through regulating the phase angle measured by the PLL. The SAC is designed to be bang-bang with only two control values

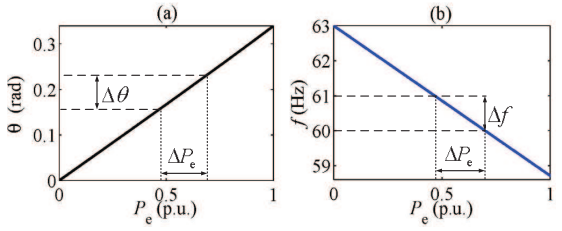

Fig. 2. (a) The active power of the DFIG $P_{\rm e}$ versus the virtual rotor angle of the DFIG θ; (b) The speed droop characteristics of synchronous generators.

[18]–[20]. In order to maintain the stable operation of the DFIG, the virtual rotor angle of the DFIG should always be positive. The input to the SAC is the load frequency deviation $f_{\rm load}-f_0$, where f_0 is the nominal frequency of the system. The switching logic of the SAC is

$$\begin{aligned} q(t) =&\mathcal{S}(e(t),\varphi_0^+-\varepsilon_0^+,\varphi_0^-+\varepsilon_0^-,q(t-)) \\ =&[e(t)\geq\varphi_0^+-\varepsilon_0^+\vee(e(t)>\varphi_0^-+\varepsilon_0^-\wedge q(t-))] \\ &q(0-)\in\{\text{true},\text{false}\} \end{aligned} \tag{3}$$

where $q(t)\in\{\text{true},\text{false}\}$ is the output of the switching logic $\mathcal{S}$, $e(t)=f_{\rm load}-f_0$ is the load frequency deviation, $\varphi_0^{\pm}$ and $\varepsilon_0^{\pm}$ are constant values used to define the error funnel $\mathcal{F}_0:=\{(t,e(t))\in\mathbb{R}_{\geq 0}\times\mathbb{R}|\varphi_0^-\leq e(t)\leq\varphi_0^+\}$, $q(t-):=\lim_{\varepsilon\to 0+}q(t-\varepsilon)$, $\vee$ represents logic operation "or", $\wedge$ represents logic operation "and", $\varphi_0^+-\varepsilon_0^+$ is the upper trigger of a switch event, $\varphi_0^-+\varepsilon_0^-$ is the lower trigger of a switch event. Hence, the switching of $q(t)$ only happens at $e(t)=\varphi_0^+-\varepsilon_0^+$ or $e(t)=\varphi_0^-+\varepsilon_0^-$. The sliding mode does not exist in the switching process of the SAC.

The control law of the SAC is given with $q(t)$ as

$$u(t)=\begin{cases} -\Delta\delta, & \text{if} \quad q(t)=\text{true} \\ \Delta\delta, & \text{if} \quad q(t)=\text{false}. \end{cases} \tag{4}$$

Referring to (3) and (4), the SAC cannot generate a neutral value, such as $u(t)=0$. However, the virtual rotor angle θ is desired to be constant in the steady state of the system. Namely, the output of the SAC should be maintained constant in the steady state of the power system, thus a conditional delay module is introduced for the SAC as

$$u(t)=\begin{cases} u(t-1), & \text{if } e(t)\in(\varphi_0^-+\varepsilon_0^-,\varphi_0^+-\varepsilon_0^+) \\ u(t), & \text{if } e(t)\leq\varphi_0^-+\varepsilon_0^-\vee e(t)\geq\varphi_0^+-\varepsilon_0^+ \end{cases} \tag{5}$$

The output of the SAC is added to the phase angle $\theta_{\rm PLL}$ measured by the PLL of the DFIG. The obtained phase angle is then used for the generation of the three phase voltage reference inputs to the PWM modules of the rotor-side and grid-side converters as depicted in Fig. 3. In this way, the active power output of the DFIG is regulated to provide frequency support to the external grid. To maintain the rotor speed being within a desirable range, the mechanical power input of the DFIG should be adjusted accordingly. This is realized by adding $K_\delta u(t)$ to the reference power set in the pitch angle control loop of the DFIG as illustrated in Fig. 3, where $P_{\rm ref\_0}$ is the reference power. To this end, the DFIG is able to provide inertia response to the external power grids and maintain the stability of itself. In the process of the primary frequency control, the re-balance of generation and load is

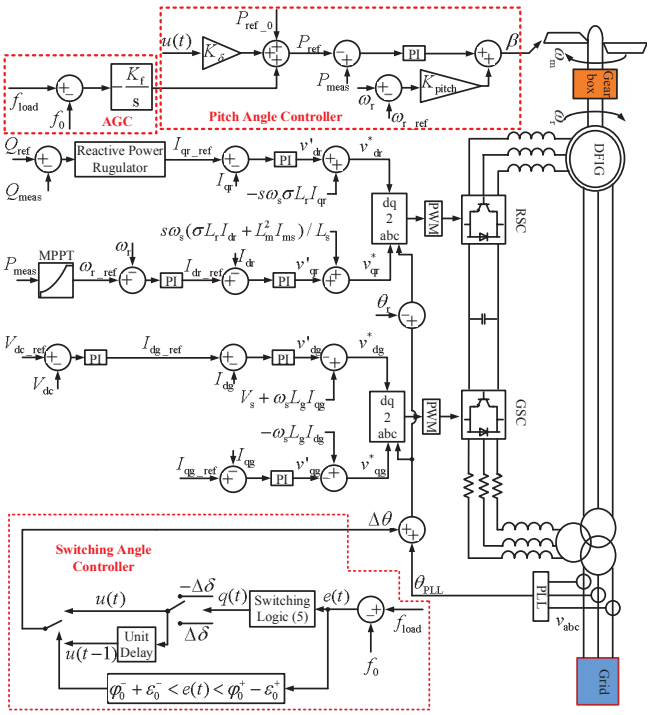

Fig. 3. The schematic of the control system of the DFIG.

achieved by the combined effort of generators and loads. Generators increase their active power outputs through the control of governors, while the power consumption of loads vary according to its speed-droop characteristics. To enable the DFIG to take part in the primary and even secondary frequency control processes of power systems, an AGC is added into the pitch angle control loop of the DFIG. The integration of system frequency deviation is added to the active power reference set in the pitch angle control loop of the DFIG as well, which is as presented in Fig. 3.

IV. Small-Signal Analysis of DFIGs with SAC and AGC

The small-signal model of the DFIG is presented in Fig. 4. The aerodynamic model of wind, a single-mass rotor model, an induction generator model [1], a pitch angle controller, and a vector controller (VC) are considered within the small-signal model. Referring to the expression of the internal voltage (2) and the schematic of the control system of the DFIG presented in Fig. 3, it has $\theta_{\rm PLL}-\theta_{\rm r}+\theta_{\rm ad}=\theta+\theta_{\rm s}$, where $\theta_{\rm PLL}$ is the phase angle measured by PLL, $\theta_{\rm s}$ is the real phase angle of the stator terminal voltage, $\theta_{\rm r}$ is the rotor angle of the DFIG, and $\theta_{\rm ad}=\arctan\frac{R_{\rm r}}{s\omega_{\rm s}L_{\rm r}}$. It follows that $\theta=\theta_{\rm PLL}+\theta_{\rm ad}-\theta_{\rm r}-\theta_{\rm s}$. Concerning $E_{\rm ms}=\frac{\sqrt{(\omega_{\rm s}L_{\rm m}R_{\rm r})^2+(s\omega_{\rm s}^2L_{\rm m}L_{\rm r})^2}V_{\rm r}}{R_{\rm r}^2+(s\omega_{\rm s}L_{\rm r})^2}$, then the active power $P_{\rm e}$ can be rewritten as

$$P_{\rm e}=\frac{E_{\rm ms}V_{\rm s}[(\frac{R_{\rm r}}{s})^2+(\omega_{\rm s}L_{\rm m})^2]\sin\theta}{\omega_{\rm s}L_{\rm ls}[(\frac{R_{\rm r}}{s})^2+(\omega_{\rm s}L_{\rm m})^2]+\omega_{\rm s}L_{\rm m}[\omega_{\rm s}^2L_{\rm lr}L_{\rm r}+(\frac{R_{\rm r}}{s})^2]} \tag{6}$$

Linearizing (6), it has

$$\Delta P_{\rm e}=\frac{\partial P_{\rm e}}{\partial E_{\rm ms}}\Delta E_{\rm ms}+\frac{\partial P_{\rm e}}{\partial\omega_{\rm s}}\Delta\omega_{\rm s}+\frac{\partial P_{\rm e}}{\partial\omega_{\rm r}}\Delta\omega_{\rm r}+\frac{\partial P_{\rm e}}{\partial\theta}\Delta\theta \tag{7}$$

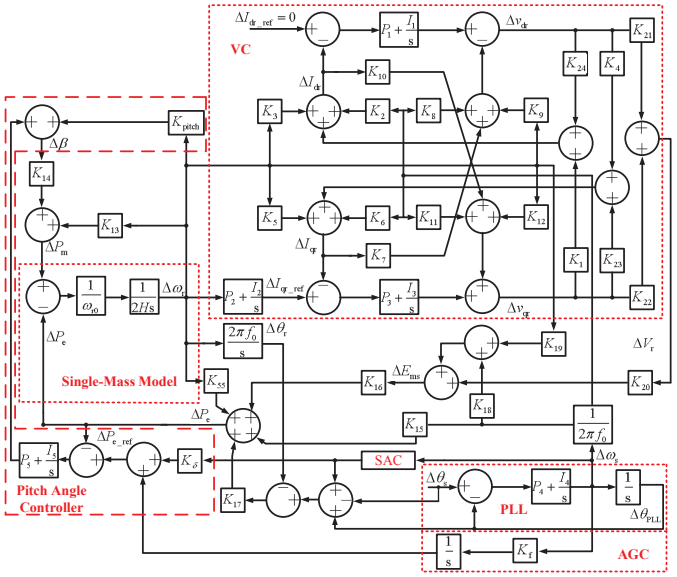

Fig. 4. The small-signal model of the DFIG.

where $\Delta\theta = \Delta\theta_{\rm PLL} + \Delta\theta_{\rm ad} - \Delta\theta_{\rm r} - \Delta\theta_{\rm s}$, and $\frac{\partial P_{\rm e}}{\partial E_{\rm ms}}$, $\frac{\partial P_{\rm e}}{\partial \omega_{\rm s}}$, $\frac{\partial P_{\rm e}}{\partial \omega_{\rm r}}$, and $\frac{\partial P_{\rm e}}{\partial \theta}$ are presented in Appendix B.

Linearize the internal voltage (2), and it can be obtained that

$$\Delta E_{\rm ms} = \frac{\partial E_{\rm ms}}{\partial v_{\rm dr}}\Delta v_{\rm dr} + \frac{\partial E_{\rm ms}}{\partial v_{\rm qr}}\Delta v_{\rm qr} + \frac{\partial E_{\rm ms}}{\partial \omega_{\rm s}}\Delta\omega_{\rm s} + \frac{\partial E_{\rm ms}}{\partial \omega_{\rm r}}\Delta\omega_{\rm r} \tag{8}$$

where $\frac{\partial E_{\rm ms}}{\partial v_{\rm dr}}$, $\frac{\partial E_{\rm ms}}{\partial v_{\rm qr}}$, $\frac{\partial E_{\rm ms}}{\partial \omega_{\rm s}}$, and $\frac{\partial E_{\rm ms}}{\partial \omega_{\rm r}}$ are illustrated in Appendix B.

With state variables chosen as $[\Delta\omega_{\rm r}\ \Delta\omega_{\rm s}]$, $\Delta v_{\rm dr}$ and $\Delta v_{\rm qr}$ can be expressed with the state variables by linearizing the VC with the DFIG model presented in [1]. Under the following assumptions,

- A.1 The reactive power reference of the DFIG is constant, thus it follows that $\Delta I_{\rm dr\_ref} = 0$. This assumption is used in the linearization of the reactive power regulator of RSC.
- A.2 The speed reference tracks the active power output slowly through the maximum power point tracking (MPPT) with a large time constant, thus it has $\Delta\omega_{\rm r\_ref} = 0$. This assumption is used in the linearization of the speed regulator of RSC.
- A.3 The external power grid is strong enough such that the magnitude of the terminal bus voltage of the DFIG is constant, i.e., $\Delta V_{\rm s} = 0$. This assumption is used in the linearization of the current control loops of RSC.

it has

$$\begin{aligned}\Delta v_{\rm qr} &= \frac{M_2({\rm s})}{M_1({\rm s})}\Delta\omega_{\rm r} + \frac{M_3({\rm s})}{M_2({\rm s})}\Delta\omega_{\rm s}\\ \Delta v_{\rm dr} &= \frac{M_6({\rm s})}{M_4({\rm s})}\Delta\omega_{\rm r} + \frac{M_5({\rm s})}{M_4({\rm s})}\Delta\omega_{\rm s}\end{aligned} \tag{9}$$

where $M_i({\rm s})(i = 1, 2, \ldots, 6)$ are given in Appendix B.

A conventional orthogonal-signal-generation based PLL is studied in this work, whose typical structure is presented in [21]. The small-signal model of the PLL is presented in Fig. 4. It can be obtained that

$$\begin{aligned}\Delta\theta_{\rm s} &= \frac{{\rm s}^2 + P_4{\rm s} + I_4}{P_4{\rm s}^2 + I_4{\rm s}}\Delta\omega_{\rm s}, \quad \Delta\theta_{\rm PLL} = \frac{1}{\rm s}\Delta\omega_{\rm s},\\ \Delta\theta_{\rm ad} &= \frac{-R_{\rm r}L_{\rm r}}{(s\omega_{\rm s}L_{\rm r})^2 + R_{\rm r}^2}(\Delta\omega_{\rm s} - \Delta\omega_{\rm r}), \quad \Delta\theta_{\rm r} = \frac{2\pi f_0}{s}\Delta\omega_{\rm r}\end{aligned} \tag{10}$$

Considering the impact of the SAC and substituting (8)-(10) into (7), (7) can be rewritten as

$$\Delta P_{\rm e} = M_{12}({\rm s})\Delta\omega_{\rm r} + M_{15}({\rm s})\Delta\omega_{\rm s} + K_{17}{\rm SAC}(\Delta\omega_{\rm s}) \tag{11}$$

where $M_{12}({\rm s})$, $M_{15}({\rm s})$, and K_{17} are shown in Appendix B.

Referring to the switching logic (3), the control law (4) of the SAC can be approximated as ${\rm SAC}(\Delta\omega_{\rm s}) \approx -\Delta\delta \cdot {\rm sgn}(\Delta\omega_{\rm s})$ on condition that $\varphi_0^+ - \varepsilon_0^+$ and $\varphi_0^- + \varepsilon_0^-$ are small enough. In order to obtain a transfer function for the control law of the SAC, a parameter η is introduced and $\eta = \Delta\delta \cdot {\rm sgn}(\Delta\omega_{\rm s})/\Delta\omega_{\rm s} = \Delta\delta/|\Delta\omega_{\rm s}|$. Then (4) can be further written as ${\rm SAC}(\Delta\omega_{\rm s}) \approx -\eta\Delta\omega_{\rm s}$. It can be noticed that η is not a constant, and it varies according to the magnitude of $\Delta\omega_{\rm s}$. Taking the SAC with parameters presented in Appendix D as an example, it has $\eta \in (0, 6]$ when system frequency excursion varies within the interval $\Delta\omega_{\rm s} \in [0.05, \infty)$.

With the above approximation, (11) can be rewritten as

$$\Delta P_{\rm e} = M_{12}({\rm s})\Delta\omega_{\rm r} + (M_{15}({\rm s}) - \eta K_{17})\Delta\omega_{\rm s}$$

where the active power response of the DFIG with respect to frequency deviation $\Delta\omega_{\rm s}$ is determined by the term $M_{15}({\rm s}) - \eta K_{17}$, whose bode diagram is as presented in Fig. 5. Six sample values of η are chosen and used for the analysis. The decrease of η represents the increase of $\Delta\omega_{\rm s}$. It can be observed that the implementation of the SAC helps to strengthen the active power response of the DFIG to system frequency excursions.

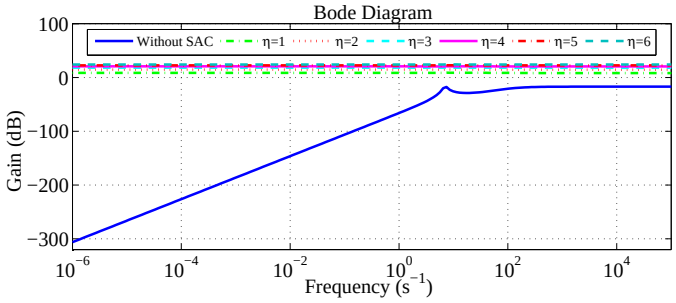

Fig. 5. The bode diagram of $M_{15}({\rm s}) - \eta K_{17}$.

For the simplicity of analysis, the dynamics of the drive train and the rotor of the induction generator are described with a single-mass model. Then rotor speed dynamics can be described with

$$\frac{1}{2H\omega_{\rm r}}(P_{\rm m} - P_{\rm e}) = \dot{\omega}_{\rm r} \tag{12}$$

where the load damping coefficient is neglected.

The mechanical power that can be extracted by the wind turbine from wind is [12]

$$P_{\rm m} = k_2 v_{\rm w}^3 C_{\rm p}(\lambda, \beta) \tag{13}$$

where k_2 is given in Appendix B, $C_{\rm p}(\lambda,\beta)=0.73[(151/\lambda_i)-0.58\beta-0.002\beta^{2.14}-13.2]e^{(-18.4/\lambda_i)}$, $1/\lambda_i=\frac{1}{\lambda-0.02\beta}-\frac{0.003}{\beta^3+1}$, $\lambda=\frac{k_1\omega_{\rm r}}{v_{\rm w}}$, and $k_1=\lambda_{C_{\rm p\_max}}v_{\rm w\_}C_{\rm pmax}/\Omega_{\rm rated}$. Linearizing (13) and taking the dynamics of the pitch angle controller, the AGC, and the SAC into consideration, it follows that

$$\Delta P_{\rm m}=M_{13}({\rm s})\Delta\omega_{\rm r}+M_{16}({\rm s})\Delta\omega_{\rm s}+M_{14}({\rm s}){\rm SAC}(\Delta\omega_{\rm s}) \quad (14)$$

where $M_{13}({\rm s})$, $M_{16}({\rm s})$, and $M_{14}({\rm s})$ are given in Appendix B.

Linearizing (12) with (11) and (14), it can be obtained that

$$\frac{\Delta\omega_{\rm r}}{\Delta\omega_{\rm s}}=\frac{M_{15}({\rm s})-M_{16}({\rm s})+\eta(K_{56}-K_{17})}{M_{13}({\rm s})-M_{12}({\rm s})-2H\omega_{\rm r}{\rm s}} \quad (15)$$

Then the bode diagrams of (15) are obtained for the DFIG with parameters given in Appendix C. Fig. 6 illustrates the frequency response of $\frac{\Delta\omega_{\rm r}}{\Delta\omega_{\rm s}}$ considering different η. As can be observed, the SAC is able to improve the response capability of rotor speed to the external system frequency deviation. The magnitude of $\frac{\Delta\omega_{\rm r}}{\Delta\omega_{\rm s}}$ decreases as the frequency deviation $\Delta\omega_{\rm s}$ increases. With the SAC, the rotating masses of the DFIG can release or restore kinetic energy to support the external system frequency. Fig. 7 presents the frequency response of $\frac{\Delta\omega_{\rm r}}{\Delta\omega_{\rm s}}$ concerning different $K_{\rm f}$. It can be noticed that the AGC mainly influence the low frequency dynamics, and it helps to reduce the low frequency and steady-state system frequency excursions.

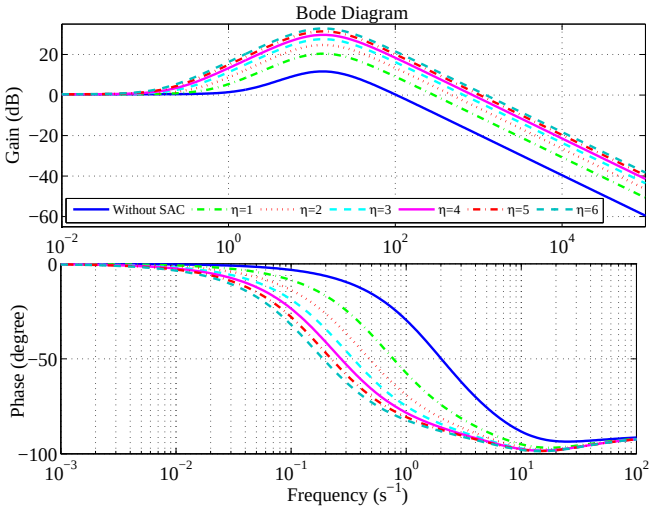

Fig. 6. The bode diagrams of $\frac{\Delta\omega_{\rm r}}{\Delta\omega_{\rm s}}$ considering different η.

V. Simulation Studies

To evaluate the control performance of the SAC and the AGC, simulation studies are carried out in a two-machine power system and a modified Kundur four-machine two-area power system, respectively. The controller parameters of the SAC and the AGC are presented in Appendix D. $\varphi_0^{\pm}$ and $\varepsilon_0^{\pm}$ are selected such that $\varphi_0^{+}-\varepsilon_0^{+}$ and $\varphi_0^{-}+\varepsilon_0^{-}$ are small values. K_δ and $K_{\rm f}$ are tuned to prevent secondary active power drop of the DFIG in the cases where the active power ouput of the DFIG is elevated by the SAC when system frequency is lower than its nominal value. In system level, the controller parameters of the RSC, GSC, SAC and AGC of the DFIG

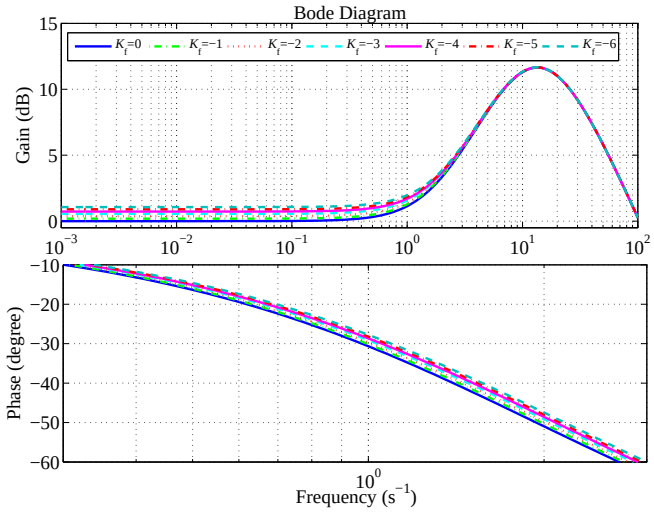

Fig. 7. The bode diagrams of $\frac{\Delta\omega_{\rm r}}{\Delta\omega_{\rm s}}$ considering different $K_{\rm f}$.

are selected to provide more damping to the rotor oscillation modes of the external power grids. The controller parameters of RSC and GSC are illustrated in Appendix D.

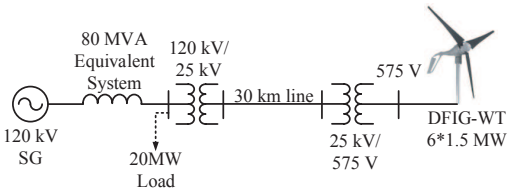

Fig. 8. The layout of the two-machine power system.

A. Dynamic Load Changes Occur in a Two-machine Power System

The layout of the two-machine power system is illustrated in Fig. 8. A 9 MW DFIG-based wind farm, which consists of 6×1.5 MW DFIG-based wind turbines, is connected to a 80 MW power system through a 25 kV transmission line and two transformers. A 20 MW load is connected to the 120 kV bus at $t=0.3$s, and it trips at $t=2$s. The wind speed subjected to the wind farm is 15 m/s.

Without the AGC and the K_δ loop presented in Fig. 3, the frequency support performance of the wind farm having only the SAC installed is studied here. Due to the dynamic load changes, system frequency drops at $t=0.3$s and overrides the nominal frequency at $t=2$s as depicted in Fig. 12 (a). It can be seen that the systems having the SAC implemented have presented less frequency excursions. Moreover, the frequency dynamics of the system is improved as the control parameter $\Delta\delta$ of the SAC increases. This is justified by Fig. 9 (b). It can be found that wind farms with the larger $\Delta\delta$ can provide more active power support to grid frequency deviations. The rotor speed of the DFIG varies in a coordinated manner with its active power output. As presented in Fig. 9 (c), the rotor decelerates to release its kinetic energy when additional active power is offered by the wind farm from $t=0.3$s. The rotor accelerates to store more kinetic energy when the active power

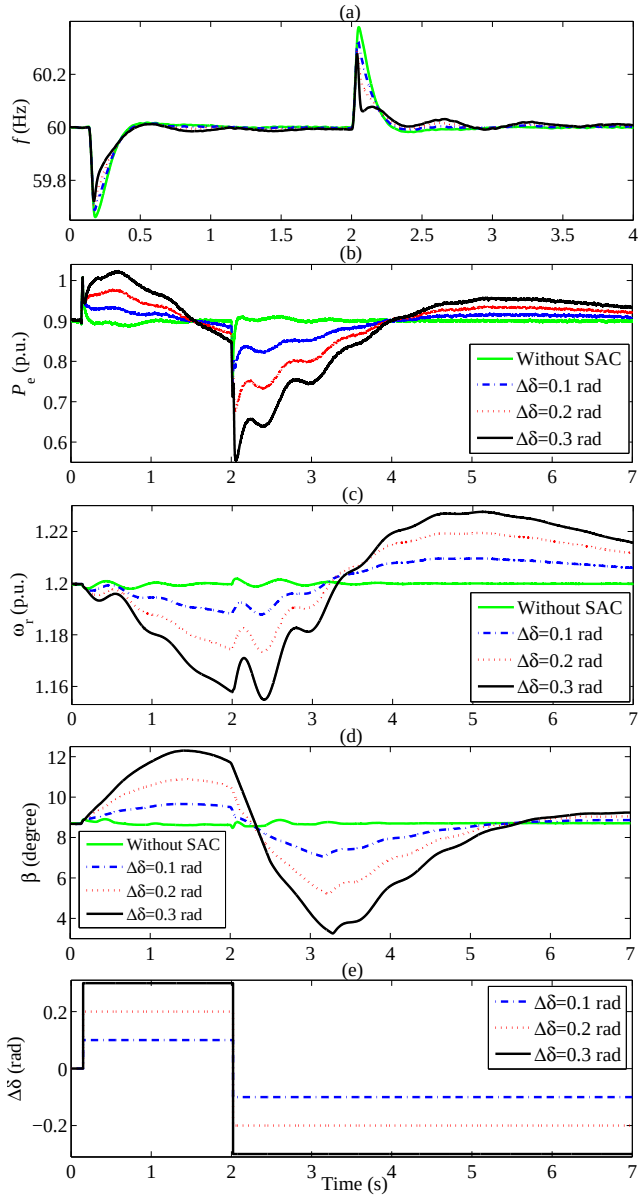

Fig. 9. Dynamics of the wind farm obtained in the case where dynamic load changes occur in a two-machine power system ((a) System frequency (b) The active power output of the wind farm (c) The rotor speed of the DFIG (d) The pitch angle of the DFIG (e) The output of the SAC).

output of the wind farm is reduced at $t = 2$s. In order to prevent the DFIG from over-speed, the pitch angle starts to increase since the rotor speed is greater than 1.2 p.u. as illustrated in Fig. 9 (d). The control signal generated by the SAC is shown in Fig. 9 (e).

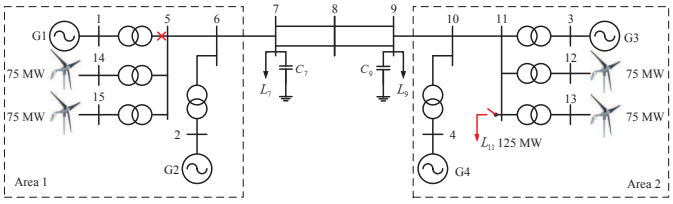

Fig. 10. The layout of the modified Kundur 4-machine 11-bus power system with four wind farms connected.

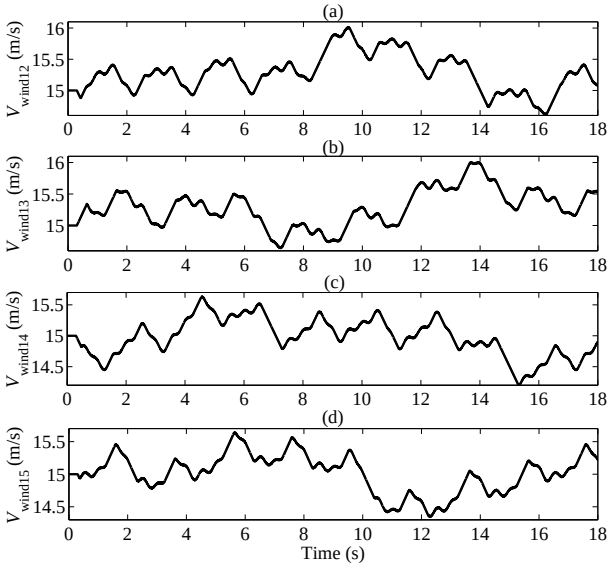

Fig. 11. The wind speed subjected to wind farm 12, 13, 14, and 15, respectively.

B. Load Increase Occurs in a Multi-machine Power System with Wind Power Penetration Under Variable Wind Speed Conditions

The frequency support performance of the DFIG controlled by the SAC and AGC is investigated here with a modified Kunder four-machine two-area power system, which is illustrated in Fig. 10. Four 75 MW wind farms, each of which is simulated with an aggregated model of 50×1.5 MW DFIGs, are connected to bus 12, 13, 14, and 15. The detailed model with all the switching process of the IGBTs of the converters considered is adopted in the modelling of DFIGs. All the DFIGs share the same configuration with parameters presented in Appendix C. The active power outputs of the four wind farms are reserved and set as 0.63 p.u., respectively. To maintain the generation and load balance, the active power outputs of G_1 and G_4 have a 94.5 MW decrease, respectively. The other configurations of the power system are the same as the original Kundur four-machine two-area system illustrated in [17]. The frequency dynamics of the system is assumed to satisfy the frequency requirements of Hydro-Québec power grids. Namely, in the steady-state, the grid frequency should be within ±0.2 Hz. Under usual operating conditions, the main system frequency is maintained within ±0.6 Hz [22].

The four 75 MW wind farms can supply 10.64% of the total system load in peak generation, which is much higher than the wind power penetration level of the state-of-the-art national stand-alone power grids [23]. For the proof-of-theory purpose as well as the time consumption and stability of the simulation model considering all the switching processes of power electronics devices, such a system is appropriate for the study in this paper. Bus 5 and bus 11 are chosen as wind power generation buses to facilitate the investigation on the impact of wind power generators in providing additional damping to the inter-area and local oscillation modes of the modified Kundur four-machine two-area power system.

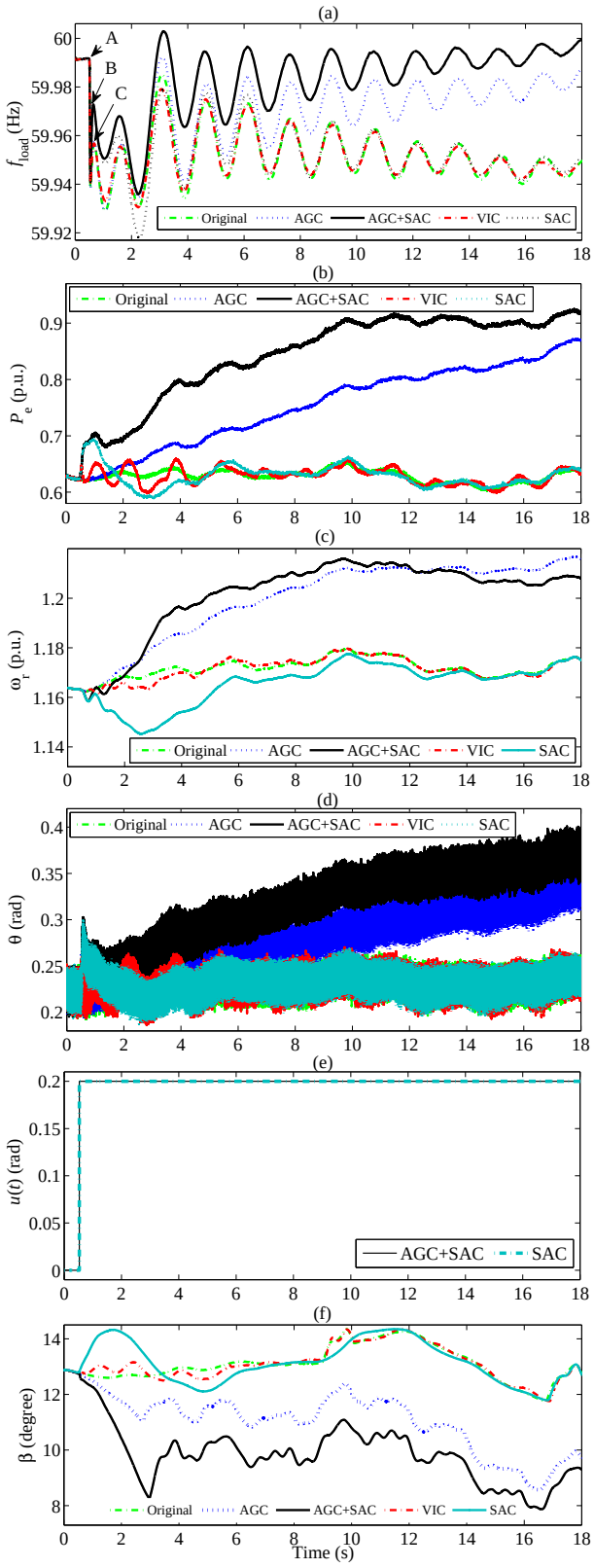

Fig. 12. The dynamics of the DFIG of wind farm 12 obtained in the case where a load increase occurs in the modified Kundur four-machine two-area power system ((a) System frequency measured by a phase-locked loop at load bus 7 (b) The active power output of the DFIG (c) The rotor speed of the DFIG (d) The virtual rotor angle of the DFIG (e) The output of the SAC installed on the DFIG (f) The pitch angle of the DFIG).

Four wind farms are operating under variable wind speed conditions [24], and the wind speed subjected to four wind farms respectively is presented in Fig. 11 (a)-(d). A 125 MW load is connected to bus 11 at $t = 0.5$s. The simulation results of the DFIG without any frequency controller are indicated by"original", those of the DFIGs having only the SAC, only the AGC, and both the SAC and the AGC installed are identified with "SAC", "AGC", and "AGC+SAC", respectively. Moreover, "VIC" denotes the simulation results of the DFIG controlled with the virtual inertia controller (VIC) proposed in [11].

The dynamics of the four wind farms are similar, thus only the dynamics of the DFIG of wind farm 12 is illustrated here. System frequency measured with a PLL at load bus 7 is shown in Fig. 12 (a). More numerical results of the system frequency are illustrated in Table I. RoCoF stands for the rate of change of frequency, which is the absolute value of the changing rate of system frequency just after a disturbance occurs. In this study, since the system frequency is measured with a PLL, the system frequency presents a sharp drop after the load increase occurs due to the voltage distortion as illustrated in Fig. 12 (a). Thus the RoCoF here is calculated with two frequency points, i.e., the pre-disturbance frequency point and the first maximum frequency point after the load increase occurs. In other words, the RoCoF here is represented with the change rate of AB and AC illustrated in Fig. 12 (a). Moreover, frequency nadir denotes the lowest system frequency during the post-disturbance stage. Settling frequency is the average value of system frequency calculated in the last oscillation cycle.

TABLE I
SYSTEM FREQUENCY PERFORMANCE INDEXES OBTAINED IN THE CASE WHERE LOAD INCREASE OCCURS

Configuration	RoCoF (Hz/s)	Frequency nadir (Hz)	Settling frequency (Hz)
Original	0.1947	59.9291	59.9476
AGC	0.1917	59.9293	59.9836
SAC	0.1040	59.9181	59.9491
AGC+SAC	0.1034	59.9358	59.9969
VIC	0.1919	59.9305	59.9478

From the results presented in Table I, all the systems having frequency controllers installed present lower RoCoF than the original system. The system having both the AGC and the SAC installed has the lowest RoCoF. Moreover, it also shows the highest frequency nadir, while the system having only the SAC implemented has the lowest frequency nadir. The frequency of the systems having only the AGC or both the SAC and the AGC installed display higher settling frequency than the systems with other control configurations.

With respect to the system having both the SAC and the AGC implemented, due to the load increase at $t = 0.5$s, the system frequency drops. When the frequency deviation is larger than 0.05 Hz, the SAC is triggered and generates a positive jump of $\Delta\delta$ as depicted in Fig. 12 (e). It follows that the virtual rotor angle θ presents a positive jump as illustrated in Fig. 12 (d). Then the active power output of the DFIG shows a positive jump as well as shown in Fig. 12 (b). Due to the K_δ and K_f loops implemented in the pitch angle controller, the

pitch angle β of the DFIG decreases continuously as depicted in Fig. 12 (f). The mechanical power input to the DFIG is then increased such that novel input-output power balance of the DFIG is achieved. The active power output and the rotor speed of the DFIG are increased and stabilized to novel equilibriums, respectively, as illustrated in Fig. 12 (b) and 12 (c).

In terms of the system having only the AGC installed, the dynamics of the active power output of the DFIG is similar to that of the DFIG having both the SAC and the AGC implemented despite of the active power jump at $t = 0.5$s as shown in Fig. 12 (b). This results in that the RoCoF of the system with only the AGC is nearly equal to that of the system with original configuration. Owning to the negative system frequency error, the AGC continuously decrease the pitch angle of the DFIG and the mechanical power input is increased accordingly. Then the active power output is elevated to offer frequency support to the external power grid as shown in Fig. 12 (b).

In terms of the system having only the SAC installed, due to the jump of its active power output at $t = 0.5$s, the lowest system frequency point is elevated during the first swing of the system as depicted in Fig. 12 (a). The increased active power output is released by the rotating masses of the DFIG as justified in Fig. 12 (c). Because of the active power feed-forward loop implemented in the pitch angle controller illustrated in Fig. 3, the pitch angle of the DFIG increases as presented in Fig. 12 (f). Consequently, the active power output of the DFIG declines, and it results in a secondary frequency drop in the external power grid, as depicted in Fig. 12 (b) and 12 (a), respectively. It follows that the system presents the lowest frequency nadir as depicted in Table I.

Regards to the system having the VIC installed, it offers relatively satisfactory frequency support performance during the initial post-disturbance stage, which can be reflected from the values of RoCoF and frequency nadir illustrated in Table I. Nevertheless, the VIC does not contribute much in the primary and secondary frequency control processes of the system, and the settling frequency of the system is lower than the systems with other configurations.

C. Modal Analysis of the Modified Kundur Four-machine Two-area Power System

Modal analysis of the modified Kundur four-machine two-area system studied in Section V-B is carried out here. A thyristor excitor and a power system stabilizer (PSS), whose parameters are shown in Appendix E, are considered in the synchronous generator model of the multi-machine power system. The oscillation modes of the system with original configuration and other configurations are illustrated in Table II. It can be observed that the AGC mainly helps to elevate rotor oscillation frequency, and the SAC mainly helps to improve the damping ratio of inter-area and local oscillation modes. Moreover, the SAC offers more damping in the case where $\eta = 6$ than in the case where $\eta = 1$, in other words, the damping effort of the SAC is more significant during the initial post-disturbance stage.

TABLE II
OSCILLATION MODES OF THE MODIFIED KUNDUR FOUR-MACHINE TWO-AREA POWER SYSTEM

Configuration		Eigenvalue/(Frequency in Hz, damping ratio)		
		Inter-area mode	Area 1 local mode	Area 2 local mode
Original		-0.173±j3.967 ($f = 0.6313$, $\xi = 0.0437$)	-1.240±j5.438 ($f = 0.8655$, $\xi = 0.2223$)	-0.682±j5.848 ($f = 0.9307$, $\xi = 0.1159$)
AGC		-0.175±j3.972 ($f = 0.6321$, $\xi = 0.0440$)	-1.242±j5.441 ($f = 0.8660$, $\xi = 0.2225$)	-0.685±j5.851 ($f = 0.9312$, $\xi = 0.1163$)
SAC	$\eta = 1$	-0.177±j3.968 ($f = 0.6315$, $\xi = 0.0447$)	-1.244±j5.440 ($f = 0.8658$, $\xi = 0.2229$)	-0.686±j5.849 ($f = 0.9310$, $\xi = 0.1165$)
	$\eta = 6$	-0.197±j3.972 ($f = 0.6322$, $\xi = 0.0496$)	-1.263±j5.449 ($f = 0.8672$, $\xi = 0.2258$)	-0.705±j5.858 ($f = 0.9323$, $\xi = 0.1194$)
AGC +SAC	$\eta = 1$	-0.178±j3.972 ($f = 0.6322$, $\xi = 0.0448$)	-1.245±j5.443 ($f = 0.8663$, $\xi = 0.2230$)	-0.687±j5.852 ($f = 0.9314$, $\xi = 0.1166$)
	$\eta = 6$	-0.198±j3.977 ($f = 0.6329$, $\xi = 0.0497$)	-1.264±j5.452 ($f = 0.8677$, $\xi = 0.2259$)	-0.706±j5.861 ($f = 0.9327$, $\xi = 0.1196$)

D. Generator Trip Occurs in a Multi-machine Power System with Wind Power Penetration Under Constant Wind Speed Conditions

The frequency control performance of the SAC and AGC is investigated in a case where generator trip occurs in the modified Kundur four-machine two-area power system as depicted in Fig. 10. The system configuration is the same as that studied in Section V-B despite that the wind farms are operating under constant wind speed conditions, and wind speed is $V_{\text{wind}} = 15$ m/s. Due to the malfunction of protection devices, generator 1 and its step-up transformer are tripped at $t = 0.5$s. The dynamics of the DFIG of wind farm 12 is illustrated in Fig. 13. Fig. 13 (a) shows the dynamics of system frequency, and more accurate evaluation with three frequency indexes are illustrated in Table III.

TABLE III
SYSTEM FREQUENCY PERFORMANCE INDEXES OBTAINED IN THE CASE WHERE GENERATOR TRIP OCCURS

Configuration	RoCoF (Hz/s)	Frequency nadir (Hz)	Settling frequency (Hz)
Original	0.5172	59.5191	59.7371
AGC	0.5163	59.5362	59.8066
SAC	0.2132	59.5459	59.7330
AGC+SAC	0.2033	59.6283	59.8089
VIC	0.4804	59.6095	59.7429

According to the results presented in Table III, the system having both the SAC and the AGC installed has the lowest RoCoF, which is justified by the active power jump of DFIG as illustrated in Fig. 13 (b). As the system frequency deviation overrides 0.05 Hz, the SAC is triggered and produces a positive step control signal as depicted in Fig. 13 (e). The virtual rotor angle and then the active power output of the DFIG are increased to compensate the active power shortage of the system as shown in Fig. 13 (d) and 13 (b), respectively. Attributed to the effort of the AGC, the pitch angle of the DFIG presents a continuous decrease after a short interval of increase since generate 1 trips as shown in Fig. 13 (f).

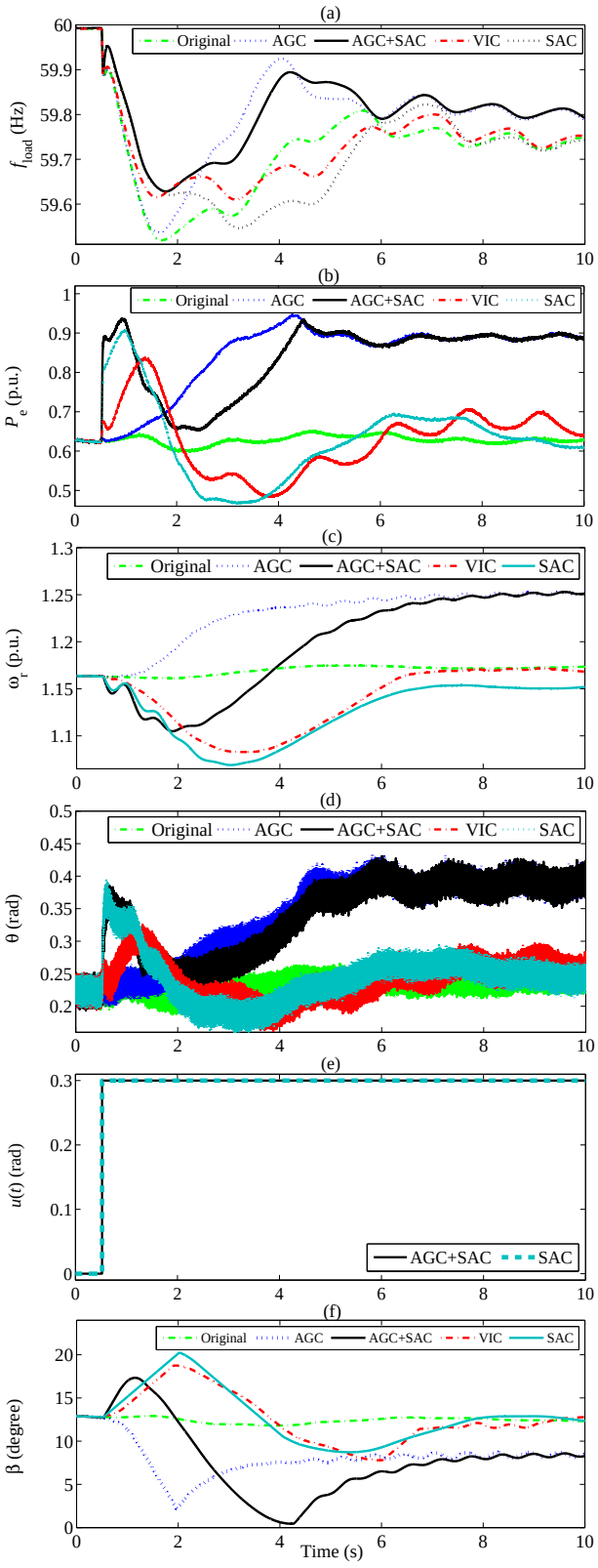

Fig. 13. The dynamics of the DFIG of wind farm 12 obtained in the case where generator trip occurs in the modified Kundur four-machine two-area power system ((a) System frequency measured by phase-locked loop at load bus 7 (b) The active power output of the DFIG (c) The rotor speed of the DFIG (d) The virtual rotor angle of the DFIG (e) The output of the SAC installed on the DFIG (f) The pitch angle of the DFIG).

It ensures that the system with both the SAC and the AGC has the highest frequency nadir. The short interval of increase of the pitch angle is caused by the active power feed-forward loop implemented in the pitch angle controller presented in Fig. 3, and it is because the active power reference cannot jump as fast as the real active power output of the DFIG. To prevent the rotor from over-speed, the pitch angle of the DFIG stars to increase after $t = 4.2$s and stabilizes to a novel value. The active power output and rotor speed of the DFIG are sequently stabilized as presented in Fig. 13 (b) and 13 (d), respectively. Moreover, according to 13 (b), the DFIGs having both the SAC and AGC or only the AGC implemented are able to provide more active power support to the external grid. These two systems thus have higher settling frequency than the system with other configurations as illustrated in Table III.

Referring to Fig. 13 (b), the systems having the SAC implemented can offer more active power support to the external grid than that with the VIC during the initial post-disturbance stage. This ensures that the systems with the SAC has a lower RoCoF than that with the VIC as shown in Table III. The DFIG having only the SAC installed shows more serious secondary active power drop, which leads to that the system with the VIC has a higher frequency nadir than that with only the SAC as illustrated in Table III. Regardless of their different dynamics, both the SAC and the VIC are able to release the kinetic energy stored in the rotating masses of the DFIG and provide inertial response to the frequency excursion of the external power grids.

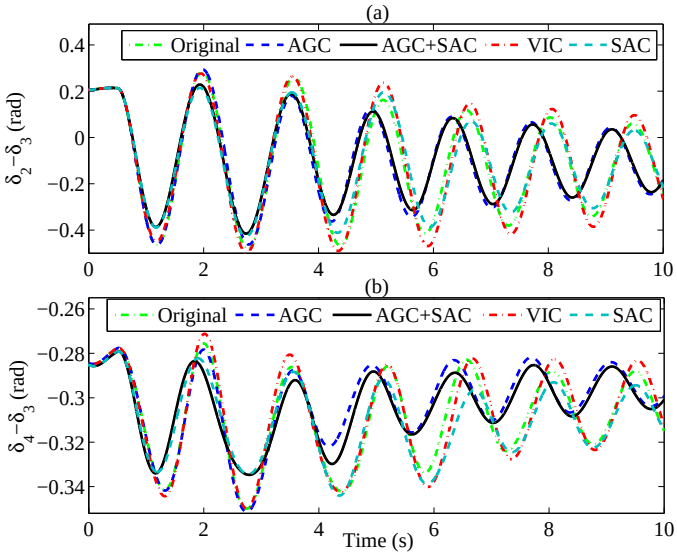

Fig. 14. The dynamics of the relative rotor angles of synchronous generators obtained in the case where a generator trip occurs in the modified Kundur four-machine two-area power system ((a) Relative rotor angle between generator 2 and generator 3 (b) Relative rotor angle between generator 4 and generator 3).

Choosing generator 3 as the slack bus of the multi-machine power system, the relative rotor angles of generator 2 and generator 4 are illustrated in Fig. 14 (a) and 14 (b), respectively. It can be seen that the systems having the SAC installed show stronger damping to the inter-area and local rotor angle

oscillations than those without the SAC. Moreover, the systems having the AGC implemented present higher oscillation frequency and stronger damping to rotor angle oscillations than those without the AGC. The simulation results meet the modal analysis of the system presented in Section V-C. Moreover, the results presented in Fig. 14 (a) and 14 (b) suggest that the SAC and the AGC can help to improve the first swing and transient stability of WPPSs.

VI. Conclusions

This paper has proposed a SAC and an AGC for the DFIG to control the frequency of DFIG-based WPPSs.

The concept of virtual rotor angle is introduced and used for the design of the SAC. The SAC functions as a bang-bang funnel controller and it is robust to system parameter changes, small-magnitude oscillations and measurement noise of system frequency. According to the small-signal analysis, the implementation of the SAC and the AGC is able to strengthen the responses of the active power output and rotor speed of DFIGs to system frequency excursions. The SAC enables the rotating masses of DFIGs to release or restore their kinetic energy to provide frequency support to the external power grids. Modal analysis of the modified Kundur four-machine two-area system suggests that the SAC and the AGC can provide additional damping to the rotor oscillation modes of the system. The AGC mainly functions to improve mode oscillation frequency, while the SAC mainly helps to increase the damping ratio of system oscillation modes.

Simulation results meet the conclusions obtained from the small-signal analysis. Due to the effort of the SAC, the virtual rotor angle of the DFIG jumps to provide fast active power support to the external power grids in the cases where system frequency excursion is larger than 0.05 Hz. The SAC with a larger $\Delta\delta$ is able to offer a larger step change of the active power output of the DFIG.

For the DFIG with both the SAC and the AGC, the active power reference set in the pitch angle controller is regulated by both of the two controllers. The SAC enables the small rapid variation of the pitch angle, while the AGC offers it slow but sustained regulation. The pitch angle of the DFIG can coordinate with the virtual rotor angle such that the secondary active power drop behavior observed in the system having only the SAC implemented is prevented. The systems having the SAC and the AGC installed have displayed the highest frequency nadir and settling frequency, as well as the lowest RoCoF among all the tested systems.

According to the RoCoF index of the studied systems, both the SAC and the VIC are able to improve system inertia. Nevertheless, the VIC cannot provide sustained active power support to the external power grids. The settling frequency of the system with the VIC is always lower than that of the systems having the AGC installed. Referring to the simulation results obtained in the case where generator trip occurs, the implementation of the SAC and the AGC helps to improve the first swing and transient stability of WPPSs as well.

Appendix A
Nomenclature

$\overrightarrow{V}_{\mathrm{s}}$	Terminal voltage (stator voltage) of the DFIG
R_{s}	Resistance of stator windings
$\overrightarrow{I}_{\mathrm{s}}$	Stator current
ω_{s}	Synchronous rotational speed (system frequency measured by PLL)
$\overrightarrow{I}_{\mathrm{r}}$	Rotor current
L_{m}	Mutual inductance of rotor-side circuit
L_{ls}	Leakage inductance of stator windings
$\overrightarrow{V}_{\mathrm{r}}$	Rotor voltage generated by the RSC
s	$s = (\omega_{\mathrm{s}} - \omega_{\mathrm{r}})/\omega_{\mathrm{s}}$ slip speed
R_{r}	Resistance of rotor windings
L_{lr}	Leakage inductance of rotor windings
$\overrightarrow{I}_{\mathrm{ms}}$	Excitation current and defined as $\overrightarrow{I}_{\mathrm{ms}} = \overrightarrow{I}_{\mathrm{s}} + \overrightarrow{I}_{\mathrm{r}}$ and I_{ms} is calculated with $I_{\mathrm{ms}} = (V_{\mathrm{s}} - R_{\mathrm{s}} I_{\mathrm{qs}})/(\omega_{\mathrm{s}} L_{\mathrm{m}})$
R_{eq}	Equivalent resistance
L_{eq}	Equivalent inductance
$\overrightarrow{E}_{\mathrm{ms}}$	Inner voltage
θ_{s}	Real phase angle of the stator voltage measured at the terminal bus of the DFIG
θ	Inner voltage
ω_{r}	Rotor speed of the DFIG
θ_{r}	Phase angle of the rotor of the DFIG
f_{load}	Load frequency measured by PLL
f_0	Nominal frequency of the power system
$\mathcal{F}_0$	Error funnel $\mathcal{F}_0 := \{(t, e(t)) \in \mathbb{R}_{\geq 0} \times \mathbb{R} \vert \varphi_0^- \leq e(t) \leq \varphi_0^+\}$
$\varphi_0^{\pm}$	Boundaries of the error funnel
$\varepsilon_0^{\pm}$	Constants used to define the error funnel
$q(t)$	Output of the switching logic of the SAC
I_{dr}	d-axis current of rotor windings
I_{qr}	q-axis current of rotor windings
I_{dg}	d-axis current of grid-side converter circuit
I_{qg}	q-axis current of grid-side converter circuit
K_{f}	Proportional gain of the AGC of the DFIG
K_δ	Proportional gain of the AGC feedback loop of the pitch angle controller of the DFIG
$P_{\mathrm{ref\_0}}$	Initial power reference point set in the pitch angle controller
P_{ref}	Power reference point set in the pitch angle controller
P_{meas}	Measured active power output of the DFIG
$\omega_{\mathrm{r\_ref}}$	Rotor speed reference
K_{pitch}	Proportional gain of the rotor speed error feedback loop of the pitch angle controller
β	Blade pitch angle of the DFIG
ω_{m}	Rotating speed of turbine blades
Q_{ref}	Reactive power output reference of the DFIG
Q_{meas}	Measured reactive power output of the DFIG
$I_{\mathrm{qr\_ref}}$	The reference of the q-axis current of rotor windings
L_{s}	Inductance of stator windings calculated with $L_{\mathrm{s}} = L_{\mathrm{ls}} + L_{\mathrm{m}}$
L_{r}	Inductance of rotor windings calculated with $L_{\mathrm{r}} = L_{\mathrm{lr}} + L_{\mathrm{m}}$
σ	Constant defined as $\sigma = 1 - L_{\mathrm{m}}^2/(L_{\mathrm{s}} L_{\mathrm{r}})$
$I_{\mathrm{dr\_ref}}$	The reference of the d-axis current of rotor windings
v_{dr}	d-axis voltage of rotor-side converter
v_{qr}	q-axis voltage of rotor-side converter
v_{dg}	d-axis voltage of grid-side converter
v_{qg}	q-axis voltage of grid-side converter
$I_{\mathrm{dg\_ref}}$	The reference of the d-axis current of grid-side filter circuit
$I_{\mathrm{qg\_ref}}$	The reference of the q-axis current of grid-side filter circuit
L_{g}	Inductance of grid-side converter filter circuit
$e(t)$	System frequency error calculated with $e(t) = f_{\mathrm{load}} - f_0$
θ_{PLL}	Phase angle measured by the PLL of the DFIG
v_{abc}	Three phase voltage of the terminal bus of the DFIG
H_{t}	Inertia constant of the single-mass model
P_{e}	Active power output of the DFIG
P_{m}	Mechanical power input of wind turbine
v_{w}	Wind speed
C_{p}	Aerodynamic coefficient of a wind turbine
C_{pmax}	The maximum of C_{p}
λ	Tip speed ratio of wind turbine
$\lambda_{C_{\mathrm{p\_max}}}$	The tip speed ratio corresponding to $C_{\mathrm{p\_max}}$
$v_{\mathrm{w\_}C_{\mathrm{pmax}}}$	The wind speed corresponding to $C_{\mathrm{p\_max}}$
Ω_{rated}	Rated mechanical rotating speed of wind turbine
K_δ	Proportional gain of the SAC loop of the pitch angle controller
K_{f}	Proportional gain of the AGC loop of the pitch angle controller
P_i, I_i	Proportional and integral gain of the PI controllers
V_{t}	Terminal voltage of synchronous generators

$V_{\mathrm{t\_ref}}$ Reference of the terminal voltage of synchronous generators
u_{PSS} Output of the PSS of synchronous generators
E_{f} Excitation voltage of synchronous generators

APPENDIX B
EXPRESSIONS OF K_i AND $M_i(\mathrm{s})$

$$K_1 = \frac{s\omega_{\mathrm{s}}\sigma L_{\mathrm{r}} L_{\mathrm{s}}^2}{L_{\mathrm{s}}(s\omega_{\mathrm{s}}\sigma L_{\mathrm{r}})^2 + (R_{\mathrm{r}}L_{\mathrm{s}})^2 + sL_{\mathrm{m}}^2 R_{\mathrm{s}} R_{\mathrm{r}}}$$

$$\begin{aligned}K_2 =&\{-R_{\mathrm{r}}\sigma L_{\mathrm{r}}[L_{\mathrm{s}}(s\omega_{\mathrm{s}}\sigma L_{\mathrm{r}})^2 + (R_{\mathrm{r}}L_{\mathrm{s}})^2 + sL_{\mathrm{m}}^2 R_{\mathrm{s}} R_{\mathrm{r}}]+\\ &2(s\omega_{\mathrm{s}})^2(\sigma L_{\mathrm{r}})^3 R_{\mathrm{r}} L_{\mathrm{s}} - s\frac{\omega_{\mathrm{r}}}{\omega_{\mathrm{s}}}\sigma R_{\mathrm{r}}^2 R_{\mathrm{s}} L_{\mathrm{r}} L_{\mathrm{m}}^2\}(sR_{\mathrm{r}}L_{\mathrm{s}}L_{\mathrm{m}}V_{\mathrm{s}}\\ &- R_{\mathrm{r}}L_{\mathrm{s}}^2 v_{\mathrm{qr}} + s\omega_{\mathrm{s}}\sigma L_{\mathrm{s}} L_{\mathrm{r}} v_{\mathrm{dr}})/[R_{\mathrm{r}}L_{\mathrm{s}}(s\omega_{\mathrm{s}}\sigma L_{\mathrm{r}}) + R_{\mathrm{r}}^3 L_{\mathrm{s}}^2\\ &+ sR_{\mathrm{s}}R_{\mathrm{r}}L_{\mathrm{m}}^2]^2 + s\omega_{\mathrm{s}}\sigma L_{\mathrm{r}}[R_{\mathrm{r}}\frac{\omega_{\mathrm{r}}}{\omega_{\mathrm{s}}^2}L_{\mathrm{s}}L_{\mathrm{m}}V_{\mathrm{s}} - \sigma L_{\mathrm{s}}L_{\mathrm{r}}v_{\mathrm{dr}}]/\\ &[R_{\mathrm{r}}L_{\mathrm{s}}(s\omega_{\mathrm{s}}\sigma L_{\mathrm{r}})^2 + R_{\mathrm{r}}^3 L_{\mathrm{s}}^2 + sR_{\mathrm{s}}R_{\mathrm{r}}^2 L_{\mathrm{m}}^2]\end{aligned}$$

$$\begin{aligned}K_3 =&\{R_{\mathrm{r}}\sigma L_{\mathrm{r}}[L_{\mathrm{s}}(s\omega_{\mathrm{s}}\sigma L_{\mathrm{r}})^2 + (R_{\mathrm{r}}L_{\mathrm{s}})^2 + sR_{\mathrm{s}}R_{\mathrm{r}}L_{\mathrm{m}}^2]-\\ &- 2(s\omega_{\mathrm{s}})^2 R_{\mathrm{r}}(\sigma L_{\mathrm{r}})^2 L_{\mathrm{s}} - sR_{\mathrm{s}}R_{\mathrm{r}}^2\sigma L_{\mathrm{r}}L_{\mathrm{m}}^2\}(sR_{\mathrm{r}}L_{\mathrm{s}}L_{\mathrm{m}}V_{\mathrm{s}}\\ &- R_{\mathrm{r}}L_{\mathrm{s}}^2 v_{\mathrm{qr}} + s\omega_{\mathrm{s}}\sigma L_{\mathrm{s}}L_{\mathrm{r}}v_{\mathrm{dr}})/[R_{\mathrm{s}}L_{\mathrm{s}}(s\omega_{\mathrm{s}}\sigma L_{\mathrm{r}})^2 + R_{\mathrm{r}}^3 L_{\mathrm{s}}^2\\ &+ sR_{\mathrm{s}}R_{\mathrm{r}}^2 L_{\mathrm{m}}^2]^2 + s\omega_{\mathrm{s}}\sigma L_{\mathrm{r}}[R_{\mathrm{r}}L_{\mathrm{s}}L_{\mathrm{m}}V_{\mathrm{s}}/\omega_{\mathrm{s}} + L_{\mathrm{s}}L_{\mathrm{r}}\sigma v_{\mathrm{dr}}]\\ &/[R_{\mathrm{r}}L_{\mathrm{s}}(s\omega_{\mathrm{s}}\sigma L_{\mathrm{r}})^2 + R_{\mathrm{r}}^3 L_{\mathrm{s}}^2 + sR_{\mathrm{s}}R_{\mathrm{r}}^2 L_{\mathrm{m}}^2]\end{aligned}$$

$$K_4 = -\frac{s\omega_{\mathrm{s}}L_{\mathrm{s}}L_{\mathrm{r}}}{L_{\mathrm{s}}(s\omega_{\mathrm{s}}\sigma L_{\mathrm{r}})^2 + (R_{\mathrm{r}}L_{\mathrm{s}})^2 + sR_{\mathrm{s}}R_{\mathrm{r}}L_{\mathrm{m}}^2}$$

$$\begin{aligned}K_5 =&[-2s\omega_{\mathrm{s}}L_{\mathrm{s}}(\sigma L_{\mathrm{r}})^2 - R_{\mathrm{s}}R_{\mathrm{r}}L_{\mathrm{m}}^2/\omega_{\mathrm{s}}](sR_{\mathrm{r}}L_{\mathrm{s}}L_{\mathrm{m}}V_{\mathrm{s}} - R_{\mathrm{r}}L_{\mathrm{s}}^2 v_{\mathrm{qr}}\\ &+ s\omega_{\mathrm{s}}L_{\mathrm{s}}\sigma L_{\mathrm{r}}v_{\mathrm{dr}})/[L_{\mathrm{s}}(s\omega_{\mathrm{s}}\sigma L_{\mathrm{r}})^2 + (R_{\mathrm{r}}L_{\mathrm{s}})^2 + sL_{\mathrm{m}}^2 R_{\mathrm{s}}R_{\mathrm{r}}]^2\\ &+ (R_{\mathrm{r}}L_{\mathrm{s}}L_{\mathrm{m}}V_{\mathrm{s}}/\omega_{\mathrm{s}} + L_{\mathrm{s}}L_{\mathrm{r}}\sigma v_{\mathrm{dr}})/[L_{\mathrm{s}}(s\omega_{\mathrm{s}}\sigma L_{\mathrm{r}})^2\\ &+ (R_{\mathrm{r}}L_{\mathrm{s}})^2 + sR_{\mathrm{s}}R_{\mathrm{r}}L_{\mathrm{m}}^2]\end{aligned}$$

$$\begin{aligned}K_6 =&[2s\omega_{\mathrm{s}}L_{\mathrm{s}}(\sigma L_{\mathrm{r}})^2 - R_{\mathrm{s}}R_{\mathrm{r}}L_{\mathrm{m}}^2\omega_{\mathrm{r}}/\omega_{\mathrm{s}}^2](sR_{\mathrm{r}}L_{\mathrm{s}}L_{\mathrm{m}}V_{\mathrm{s}} - R_{\mathrm{r}}L_{\mathrm{s}}^2 v_{\mathrm{qr}}\\ &+ s\omega_{\mathrm{s}}L_{\mathrm{s}}\sigma L_{\mathrm{r}}v_{\mathrm{dr}})/[L_{\mathrm{s}}(s\omega_{\mathrm{s}}\sigma L_{\mathrm{r}})^2 + (R_{\mathrm{r}}L_{\mathrm{s}})^2 + sL_{\mathrm{m}}^2 R_{\mathrm{s}}R_{\mathrm{r}}]^2\\ &+ (R_{\mathrm{r}}L_{\mathrm{s}}L_{\mathrm{m}}V_{\mathrm{s}}\omega_{\mathrm{r}}/\omega_{\mathrm{s}}^2 - L_{\mathrm{s}}L_{\mathrm{r}}\sigma v_{\mathrm{dr}})/[L_{\mathrm{s}}(s\omega_{\mathrm{s}}\sigma L_{\mathrm{r}})^2\\ &+ (R_{\mathrm{r}}L_{\mathrm{s}})^2 + sR_{\mathrm{s}}R_{\mathrm{r}}L_{\mathrm{m}}^2]\end{aligned}$$

$$K_7 = s\omega_{\mathrm{s}}\sigma L_{\mathrm{r}}, \quad K_8 = \sigma L_{\mathrm{r}} i_{\mathrm{qr}}$$

$$K_9 = -\sigma L_{\mathrm{r}} i_{\mathrm{qr}}, \quad K_{10} = \frac{s\omega_{\mathrm{s}}\sigma L_{\mathrm{r}}}{L_{\mathrm{s}}}$$

$$K_{11} = (\omega_{\mathrm{s}}^2\sigma L_{\mathrm{r}} I_{\mathrm{dr}} + \omega_{\mathrm{r}} L_{\mathrm{m}} V_{\mathrm{s}})/(\omega_{\mathrm{s}}^2 L_{\mathrm{s}})$$

$$K_{12} = -(\omega_{\mathrm{s}}\sigma L_{\mathrm{r}} I_{\mathrm{dr}} + L_{\mathrm{m}} V_{\mathrm{s}})/(\omega_{\mathrm{s}} L_{\mathrm{s}})$$

$$K_{13} = \frac{\partial P_{\mathrm{m}}}{\partial \omega_{\mathrm{r}}} = \frac{k_2 v_{\mathrm{w}}^3 \lambda}{\omega_{\mathrm{r}}}\frac{\partial C_{\mathrm{p}}(\lambda,\beta)}{\partial \lambda}$$

$$K_{14} = \frac{\partial P_{\mathrm{m}}}{\partial \beta} = k_2 v_{\mathrm{w}}^3 \frac{\partial C_{\mathrm{p}}(\lambda,\beta)}{\partial \beta}$$

$$\frac{\partial P_{\mathrm{e}}}{\partial \omega_{\mathrm{s}}} = K_{15}, \quad \frac{\partial P_{\mathrm{e}}}{\partial E_{\mathrm{ms}}} = K_{16}, \quad \frac{\partial P_{\mathrm{e}}}{\partial \theta} = K_{17}, \quad \frac{\partial P_{\mathrm{e}}}{\partial \omega_{\mathrm{r}}} = K_{55}$$

$$\begin{aligned}K_{15} =&\{E_{\mathrm{ms}}V_{\mathrm{s}}\sin\theta(-\frac{R_{\mathrm{r}}^2\omega_{\mathrm{r}}}{s^3\omega_{\mathrm{s}}^2} + 2L_{\mathrm{m}}^2\omega_{\mathrm{s}})\{\omega_{\mathrm{s}}L_{\mathrm{ls}}[(\frac{R_{\mathrm{r}}}{s})^2+\\ &(\omega_{\mathrm{s}}L_{\mathrm{m}})^2] + \omega_{\mathrm{s}}L_{\mathrm{m}}[\omega_{\mathrm{s}}^2 L_{\mathrm{lr}}L_{\mathrm{r}} + (\frac{R_{\mathrm{r}}}{s})^2]\} - E_{\mathrm{ms}}V_{\mathrm{s}}\sin\theta\\ &\left[(\frac{R_{\mathrm{r}}}{s})^2 + (\omega_{\mathrm{s}}L_{\mathrm{m}})^2\right]\{L_{\mathrm{ls}}\left[(\frac{R_{\mathrm{r}}}{s})^2 + (\omega_{\mathrm{s}}L_{\mathrm{m}})^2\right] + \omega_{\mathrm{s}}L_{\mathrm{ls}}\\ &\left[-\frac{R_{\mathrm{r}}^2\omega_{\mathrm{r}}}{s^3\omega_{\mathrm{s}}^2} + 2L_{\mathrm{m}}^2\omega_{\mathrm{s}}\right] + L_{\mathrm{m}}\left[\omega_{\mathrm{s}}^2 L_{\mathrm{lr}}L_{\mathrm{r}} + (\frac{R_{\mathrm{r}}}{s})^2\right] + \omega_{\mathrm{s}}L_{\mathrm{m}}\\ &(-\frac{R_{\mathrm{r}}^2\omega_{\mathrm{r}}}{s^3\omega_{\mathrm{s}}^2} + 2\omega_{\mathrm{s}}L_{\mathrm{lr}}L_{\mathrm{r}})\}\}/\{\omega_{\mathrm{s}}L_{\mathrm{ls}}\left[(\frac{R_{\mathrm{r}}}{s})^2 + (\omega_{\mathrm{s}}L_{\mathrm{m}})^2\right] +\\ &\omega_{\mathrm{s}}L_{\mathrm{m}}\left[(\frac{R_{\mathrm{r}}}{s})^2 + \omega_{\mathrm{s}}^2 L_{\mathrm{lr}}L_{\mathrm{r}}\right]\}^2\end{aligned}$$

$$\begin{aligned}K_{55} =&\frac{2E_{\mathrm{ms}}V_{\mathrm{s}}R_{\mathrm{r}}\sin\theta}{\omega_{\mathrm{s}}s^3}\{\omega_{\mathrm{s}}L_{\mathrm{ls}}\left[(\frac{R_{\mathrm{r}}}{s})^2 + (\omega_{\mathrm{s}}L_{\mathrm{m}})^2\right] + \omega_{\mathrm{s}}L_{\mathrm{m}}\\ &\left[(\frac{R_{\mathrm{r}}}{s})^2 + \omega_{\mathrm{s}}^2 L_{\mathrm{lr}}L_{\mathrm{r}}\right]\} - \frac{2R_{\mathrm{r}}L_{\mathrm{s}}E_{\mathrm{ms}}V_{\mathrm{s}}\sin\theta}{s^3}[(\frac{R_{\mathrm{r}}}{s})^2 + (\omega_{\mathrm{s}}L_{\mathrm{m}})^2]\\ &/\{\omega_{\mathrm{s}}L_{\mathrm{ls}}\left[(\frac{R_{\mathrm{r}}}{s})^2 + (\omega_{\mathrm{s}}L_{\mathrm{m}})^2\right] + \omega_{\mathrm{s}}L_{\mathrm{m}}\left[(\frac{R_{\mathrm{r}}}{s})^2 + \omega_{\mathrm{s}}^2 L_{\mathrm{lr}}L_{\mathrm{r}}\right]\}^2\end{aligned}$$

$$K_{16} = \frac{V_{\mathrm{s}}\sin\theta\left[(\frac{R_{\mathrm{r}}}{s})^2 + (\omega_{\mathrm{s}}L_{\mathrm{m}})^2\right]}{\omega_{\mathrm{s}}L_{\mathrm{ls}}\left[(\frac{R_{\mathrm{r}}}{s})^2 + (\omega_{\mathrm{s}}L_{\mathrm{m}})^2\right] + \omega_{\mathrm{s}}L_{\mathrm{m}}\left[(\frac{R_{\mathrm{r}}}{s})^2 + \omega_{\mathrm{s}}^2 L_{\mathrm{lr}}L_{\mathrm{r}}\right]}$$

$$K_{17} = \frac{E_{\mathrm{ms}}V_{\mathrm{s}}\left[(\frac{R_{\mathrm{r}}}{s})^2 + (\omega_{\mathrm{s}}L_{\mathrm{m}})^2\right]\cos\theta}{\omega_{\mathrm{s}}L_{\mathrm{ls}}\left[(\frac{R_{\mathrm{r}}}{s})^2 + (\omega_{\mathrm{s}}L_{\mathrm{m}})^2\right] + \omega_{\mathrm{s}}L_{\mathrm{m}}\left[(\frac{R_{\mathrm{r}}}{s})^2 + \omega_{\mathrm{s}}^2 L_{\mathrm{ls}}L_{\mathrm{r}}\right]}$$

$$\frac{\partial E_{\mathrm{ms}}}{\partial v_{\mathrm{dr}}} = K_{20}K_{21}, \ \frac{\partial E_{\mathrm{ms}}}{\partial v_{\mathrm{qr}}} = K_{20}K_{22}, \ \frac{\partial E_{\mathrm{ms}}}{\partial \omega_{\mathrm{s}}} = K_{18}, \ \frac{\partial E_{\mathrm{ms}}}{\partial \omega_{\mathrm{r}}} = K_{19}$$

$$\begin{aligned}K_{18} =&\{V_{\mathrm{r}}s\omega_{\mathrm{s}}^2 L_{\mathrm{m}}^2 L_{\mathrm{r}}^2[R_{\mathrm{r}}^2 + (s\omega_{\mathrm{s}}L_{\mathrm{r}})^2](2s\omega_{\mathrm{s}} - \omega_{\mathrm{r}})\\ &- 2V_{\mathrm{r}}s\omega_{\mathrm{s}}L_{\mathrm{r}}^2[(s\omega_{\mathrm{s}}^2 L_{\mathrm{m}}L_{\mathrm{r}})^2 + (\omega_{\mathrm{s}}L_{\mathrm{m}}R_{\mathrm{r}})^2](s - \frac{\omega_{\mathrm{r}}}{\omega_{\mathrm{s}}})\}\\ &/\{[R_{\mathrm{r}}^2 + (s\omega_{\mathrm{s}}L_{\mathrm{r}})^2]^2\sqrt{(s\omega_{\mathrm{s}}^2 L_{\mathrm{m}}L_{\mathrm{r}})^2 + (\omega_{\mathrm{s}}L_{\mathrm{m}}R_{\mathrm{r}})^2}\}\end{aligned}$$

$$\begin{aligned}K_{19} =&\{2V_{\mathrm{r}}s\omega_{\mathrm{s}}L_{\mathrm{r}}^2[(s\omega_{\mathrm{s}}^2 L_{\mathrm{m}}L_{\mathrm{r}})^2 + (\omega_{\mathrm{s}}L_{\mathrm{m}}R_{\mathrm{r}})^2]\\ &- V_{\mathrm{r}}s\omega_{\mathrm{s}}^3 L_{\mathrm{m}}^2 L_{\mathrm{r}}^2[R_{\mathrm{r}}^2 + (s\omega_{\mathrm{s}}L_{\mathrm{r}})^2]\}/\\ &\{[R_{\mathrm{r}}^2 + (s\omega_{\mathrm{s}}L_{\mathrm{r}})^2]^2\sqrt{(s\omega_{\mathrm{s}}^2 L_{\mathrm{m}}L_{\mathrm{r}})^2 + (\omega_{\mathrm{s}}L_{\mathrm{m}}R_{\mathrm{r}})^2}\}\end{aligned}$$

$$K_{20} = \frac{\sqrt{(s\omega_{\mathrm{s}}^2 L_{\mathrm{m}}L_{\mathrm{r}})^2 + (\omega_{\mathrm{s}}L_{\mathrm{m}}R_{\mathrm{r}})^2}}{R_{\mathrm{r}}^2 + (s\omega_{\mathrm{s}}L_{\mathrm{r}})^2}$$

$$K_{21} = \frac{v_{\mathrm{dr}}}{V_{\mathrm{r}}}, \quad K_{22} = \frac{v_{\mathrm{qr}}}{V_{\mathrm{r}}}, \quad k_2 = \frac{0.75}{v_{\mathrm{w\_max}}^3 C_{\mathrm{p\_max}}}$$

$$\begin{aligned}M_1(\mathrm{s}) =&[1 + K_{24}\frac{P_1\mathrm{s} + I_1}{\mathrm{s}} + K_4K_7][1 - K_1K_{10} + K23\frac{P_3\mathrm{s} + I_3}{\mathrm{s}}]\\ &+ [K_{10}K_{24} - K_4\frac{P_3\mathrm{s} + I_3}{\mathrm{s}}][K_1\frac{P_1\mathrm{s} + I_1}{\mathrm{s}} + K_7K_{23}]\end{aligned}$$

$$\begin{aligned}M_2(\mathrm{s}) =&[K_3K_{10} + K_{12} + \frac{(P_3\mathrm{s} + I_3)(P_2\mathrm{s} + I_2)}{\mathrm{s}^2} - K_5\frac{P_3\mathrm{s} + I_3}{\mathrm{s}}]\cdot\\ &[1 + K_4K_7 + K_{24}\frac{P_1\mathrm{s} + I_1}{\mathrm{s}}]-\\ &[K_{10}K_{24} - K_4\frac{P_3\mathrm{s} + I_3}{\mathrm{s}}][K_3\frac{P_1\mathrm{s} + I_1}{\mathrm{s}} + K_5K_7 + K_9]\end{aligned}$$

$$\begin{aligned}M_3(\mathrm{s}) =&[1 + K_{24}\frac{P_1\mathrm{s} + I_1}{\mathrm{s}} + K_4K_7][K_2K_{10} + K_{11} - K_6\frac{P_3\mathrm{s} + I_3}{\mathrm{s}}]\\ &- [K_{10}K_{24} - K_4\frac{P_3\mathrm{s} + I_3}{\mathrm{s}}][K_2\frac{P_1\mathrm{s} + I_1}{\mathrm{s}} + K_8 + K_6K_7]\end{aligned}$$

$$M_4(\mathrm{s}) = [1 + K_{24}\frac{P_1\mathrm{s} + I_1}{\mathrm{s}} + K_4K_7][K_{10}K_{24} - K_4\frac{P_3\mathrm{s} + I_3}{\mathrm{s}}]$$

$$\begin{aligned}M_5(\mathrm{s}) =&[1 + K_4K_7 + K_{24}\frac{(P_1\mathrm{s} + I_1)}{\mathrm{s}}][1 - K_1K_{10} + K_{23}\cdot\\ &\frac{(P_3\mathrm{s} + I_3)}{\mathrm{s}}]\frac{M_3(\mathrm{s})}{M_1(\mathrm{s})} - [1 + K4K_7 + K_{24}\frac{P_1\mathrm{s} + I_1}{\mathrm{s}}]\cdot\\ &[K_2K_{10} + K_{11} - K_6\frac{P_3\mathrm{s} + I_3}{\mathrm{s}}]\end{aligned}$$

$$\begin{aligned}M_6(\mathrm{s}) =&[1 + K_4K_7 + K_{24}\frac{P_1\mathrm{s} + I_1}{\mathrm{s}}][1 - K_1K_{10} + K_{23}\frac{P_3\mathrm{s} + I_3}{\mathrm{s}}]\\ &\frac{M_2(\mathrm{s})}{M_1(\mathrm{s})} - [K_3K_{10} + K_{12} + \frac{(P_3\mathrm{s} + I_3)(P_2\mathrm{s} + I_2)}{\mathrm{s}^2}\\ &- K_5\frac{P_3\mathrm{s} + I_3}{\mathrm{s}})][1 + K_4K_7 + K_{24}(P_1 + \frac{I_1}{\mathrm{s}})]\end{aligned}$$

$$M_7(\mathrm{s}) = K_{20}K_{21}\frac{M_6(\mathrm{s})}{M_4(\mathrm{s})} + K_{20}K_{22}\frac{M_2(\mathrm{s})}{M_1(\mathrm{s})} + K_{19}$$

$$M_8(\mathrm{s}) = K_{20}K_{21}\frac{M_5(\mathrm{s})}{M_4(\mathrm{s})} + K_{20}K_{22}\frac{M_3(\mathrm{s})}{M_1(\mathrm{s})} + K_{18}$$

$$M_9(\mathrm{s}) = \frac{P_4\mathrm{s} + I_4}{\mathrm{s}^2 + P_4\mathrm{s} + I_4}, \quad M_{10}(\mathrm{s}) = \mathrm{s}M_9(\mathrm{s})$$

$$M_{11}(\mathrm{s}) = K_{17}M_9(\mathrm{s}) - K_{17} + [K_{16}M_8(\mathrm{s}) + K_{15} + K_{17}K_{25}]M_{10}(\mathrm{s})$$

$$M_{12}(\mathrm{s}) = -\frac{2\pi f_0 K_{17}}{\mathrm{s}} + K_{16}M_7(\mathrm{s}) - K_{17}K_{25}$$

$$M_{15}(\mathrm{s}) = \frac{M_{11}(\mathrm{s})}{M_{12}(\mathrm{s})}$$

$$M_{13}(\mathrm{s}) = K_{13} + K_{14}K_{\mathrm{pitch}} + K_{14}M_{12}(\mathrm{s})(P_5 + \frac{I_5}{\mathrm{s}})$$

$$M_{14}(\mathrm{s}) = K_{14}K_{17}(P_5 + \frac{I_5}{\mathrm{s}}) - K_{14}K_\delta(P_5 + \frac{I_5}{\mathrm{s}})$$

$$M_{16}(\mathrm{s}) = K_{14}(P_5 + \frac{I_5}{\mathrm{s}})[\frac{M_{11}(\mathrm{s})}{M_{10}(\mathrm{s})} - \frac{K_{\mathrm{f}}}{\mathrm{s}}]$$

$$K_{23}=\frac{L_{\rm s}^2R_{\rm r}}{L_{\rm s}(s\omega_{\rm s}\sigma L_{\rm r})^2+(R_{\rm r}L_{\rm s})^2+sR_{\rm s}R_{\rm r}L_{\rm m}^2}$$
$$K_{24}=\frac{1}{R_{\rm r}}-\frac{L_{\rm s}(s\omega_{\rm s}\sigma L_{\rm r})^2}{R_{\rm r}[L_{\rm s}(s\omega_{\rm s}\sigma L_{\rm r})^2+(R_{\rm r}L_{\rm s})^2+sR_{\rm s}R_{\rm r}L_{\rm m}^2]}$$
$$K_{25}=\frac{-R_{\rm r}L_{\rm r}}{(s\omega_{\rm s}L_{\rm r})^2+R_{\rm r}^2}$$
$$K_{53}=(K_{14}-1)(K_{15}+K_{17}K_{25})+\eta[K_{14}(K_{17}-K_\delta)-K_{17}]+(K_{14}-1)K_{16}K_{18}$$
$$K_{54}=-K_4K_{24}I_1I_3[(K_{14}-1)K_{17}-K_{14}K_{\rm f}]$$
$$K_{26}=K_{53}(1+K_4K_7+K_{24}P_1)(K_{10}K_{24}-K_4P_3)-\frac{1}{2\pi f_0}\cdot(K_{14}-1)K_{16}K_{20}K_{21}(1+K_4K_7+K_{24}P_1)(K_2K_{10}+K_{11}-K_6P_3)$$
$$K_{27}=K_{53}[K_{24}I_1(K_{10}K_{24}-K_4P_3)-K_4I_3(1+K_4K_7+K_{24}P_1)]+[(K_{14}-1)K_{17}-K_{14}K_{\rm f}](1+K_4K_7+K_{24}P_1)(K_{10}K_{24}-K_4P_3)-\frac{1}{2\pi f_0}(K_{14}-1)K_{16}K_{20}K_{21}[K_{24}I_1(K_2K_{10}+K_{11}-K_6P_3)-K_6I_3(1+K_4K_7+K_{24}P_1)]$$
$$K_{28}=-K_4K_{24}K_{53}I_1I_3+[(K_{14}-1)K_{17}-K_{14}K_{\rm f}][K_{24}I_1(K_{10}K_{24}-K_4P_3)-K_4I_3(1+K_4K_7+K_{24}P_1)]+\frac{1}{2\pi f_0}\cdot(K_{14}-1)K_6K_{16}K_{20}K_{21}K_{24}I_1I_3$$
$$K_{29}=(1+K_4K_7+K_{24}P_1)(1-K_1K_{10}+K_{23}P_3)+(K_{10}K_{24}-K_4P_3)(K_1P_1+K_7K_{23})$$
$$K_{30}=K_{24}I_1(1-K_1K_{10}+K_{23}P_3)+K_{23}I_3(1+K_4K_7+K_{24}P_1)+K_1I_1(K_{10}K_{24}-K_4P_3)-K_4I_3(K_1P_1+K_7K_{23})$$
$$K_{31}=K_{23}K_{24}I_1I_3-K_1K_4I_1I_3$$
$$K_{32}=\frac{1}{2\pi f_0}(K_{14}-1)K_{16}K_{20}K_{21}(1+K_4K_7+K_{24}P_1)(1-K_1K_{10}+K_{23}P_3)+\frac{1}{2\pi f_0}(K_{14}-1)K_{16}K_{20}K_{22}(1+K_4K_7+K_{24}P_1)(K_{10}K_{24}-K_4P_3)$$
$$K_{33}=\frac{1}{2\pi f_0}(K_{14}-1)K_{16}K_{20}K_{21}[K_{23}I_3(1+K_4K_7+K_{24}P_1)+K_{24}I_1(1-K_1K_{10}+K_{23}P_3)]+\frac{1}{2\pi f_0}(K_{14}-1)K_{16}K_{20}K_{22}[K_{24}I_1(K_{10}K_{24}-K_4P_3)-K_4I_3(1+K_4K_7+K_{24}P_1)]$$
$$K_{34}=\frac{1}{2\pi f_0}(K_{14}-1)K_{16}K_{20}(K_{21}K_{23}K_{24}I_1I_3-K_4K_{22}K_{24}I_1I_3)$$
$$K_{35}=(1+K_4K_7+K_{24}P_1)(K_2K_{10}+K_{11}-K_6P_3)-(K_{10}K_{24}-K_4P_3)(K_8+K_6K_7+K_2P_1)$$
$$K_{36}=K_{24}I_1(K_2K_{10}+K_{11}-K_6P_3)-K_6I_3(1+K_4K_7+K_{24}P_1)-K_2I_1(K_{10}K_{24}-K_4P_3)+K_4I_3(K_8+K_6K_7+K_2P_1)$$
$$K_{37}=K_2K_4I_1I_3-K_6K_{24}I_1I_3$$
$$K_{38}=2H\omega_{\rm r}(1+K_4K_7+K_{24}P_1)(K_{10}K_{24}-K_4P_3)$$
$$K_{39}=2H\omega_{\rm r}[K_{24}I_1(K_{10}K_{24}-K_4P_3)-K_4I_3(1+K_4K_7+K_{24}P_1)]+[-K_{13}-K_{14}K_{\rm pitch}+(1-K_{14})K_{16}K_{19}](1+K_4K_7+K_{24}P_1)(K_{10}K_{24}-K_4P_3)-(1-K_{14})K_{16}K_{20}K_{21}\cdot(1+K_4K_7+K_{24}P_1)(K_3K_{10}+K_{12}+P_2P_3-K_5P_3)$$
$$K_{40}=-2H\omega_{\rm r}K_4K_{24}I_1I_3+[-K_{13}-K_{14}K_{\rm pitch}+(1-K_{14})K_{16}K_{19}][K_{24}I_1(K_{10}K_{24}-K_4P_3)-K_4I_3(1+K_4K_7+K_{24}P_1)]+2\pi f_0K_{17}(K_{14}-1)(1+K_4K_7+K_{24}P_1)(K_{10}K_{24}-K_4P_3)-(1-K_{14})K_{16}K_{20}K_{21}[(1+K_4K_7+K_{24}P_1)\cdot(P_3I_2+P_2I_3-K_5I_3)+K_{24}I_1(K_3K_{10}+K_{12}+P_2P_3-K_5P_3)]$$
$$K_{41}=-K_4K_{24}I_1I_3[-K_{13}-K_{14}K_{\rm pitch}+(1-K_{14})K_{16}K_{19}]+2\pi f_0K_{17}(K_{14}-1)[K_{24}I_1(K_{10}K_{24}-K_4P_3)-K_4I_3(1+K_4K_7+K_{24}P_1)]-(1-K_{14})K_{16}K_{20}K_{21}[I_2I_3(1+K_4K_7+K_{24}P_1)+K_{24}I_1(P_3I_2+P_2I_3-K_5I_3)]$$
$$K_{42}=-2\pi f_0K_4K_{17}(K_{14}-1)K_{24}I_1I_3-(1-K_{14})K_{16}K_{20}K_{21}K_{24}I_1I_2I_3$$
$$K_{43}=(1+K_4K_7+K_{24}P_1)(1-K_1K_{10}+K_{23}P_3)+(K_{10}K_{24}-K_4P_3)(K_7K_23+K_1P_1)$$
$$K_{44}=I_3K_{23}(1+K_4K_7+K_{24}P_1)+K_{24}I_1(1-K_1K_{10}+K_{23}P_3)+K_1I_1(K_{10}K_{24}-K_4P_3)-K_4I_3(K_7K_{23}+K_1P_1)$$
$$K_{45}=K_{23}K_{24}I_1I_3-K_1K_4I_1I_3$$
$$K_{46}=K_{16}K_{20}K_{21}(1-K_{14})(1+K_4K_7+K_{24}P_1)(1-K_1K_{10}+K_{23}P_3)$$
$$K_{47}=K_{16}K_{20}K_{21}(1-K_{14})[K_{23}I_3(1+K_4K_7+K_{24}P_1)+K_{24}I_1(1-K_1K_{10}+K_{23}P_3)]$$
$$K_{48}=K_{16}K_{20}K_{21}K_{23}K_{24}(1-K_{14})I_1I_3$$
$$K_{49}=(1+K_4K_7+K_{24}P_1)(K_3K_{10}+K_{12}+P_2P_3-K_5P_3)-(K_{10}K_{24}-K_4P_3)(K_5K_7+K_9+K_3P_1)$$
$$K_{50}=(1+K_4K_7+K_{24}P_1)(P_3I_2+P_2I_3-K_5I_3)+K_{24}I_1(K_3K_{10}+K_{12}+P_2P_3-K_5P_3)-K_3I_1(K_{10}K_{24}-K_4P_3)+K_4I_3(K_5K_7+K_9+K_3P_1)$$
$$K_{51}=I_2I_3(1+K_4K_7+K_{24}P_1)+K_{24}I_1(P_3I_2+P_2I_3-K_5I_3)+K_3K_4I_1I_3$$
$$K_{52}=K_{24}I_1I_2I_3$$

APPENDIX C
PARAMETERS OF THE DFIG

Nominal active power $P_{\rm n}=1.5$MW, nominal voltage of stator windings $V_{\rm s_nom}=575$V, nominal voltage of rotor windings $V_{\rm r_nom}=1975$V, nominal frequency $f=60$Hz, $R_{\rm s}$=0.023 p.u., $L_{\rm ls}$=0.18 p.u., $R_{\rm r}$=0.016 p.u., $L_{\rm lr}$=0.16 p.u., $L_{\rm m}=2.9$ p.u., inertia constant of induction generator $H_1=0.685$s, pairs of poles $p=3$, grid-side converter maximum current (pu of generator nominal current) $I_{\rm g_max}=0.8$p.u., grid-side coupling resistance $R_{\rm g}=0.003$ p.u., grid-side coupling inductance $L_{\rm g}=0.3$ p.u., nominal DC bus voltage $V_{\rm dc_nom}=1150$V, DC bus capacitor $C=$ 1e-2 F, wind speed at $C_{\rm p\_max}$ is 11 m/s, nominal mechanical output power is 1.5e6 W, inertia constant of wind turbine $H_2=4.32$s, turbine initial speed (pu of nominal speed) $\omega_{\rm m}=1.2$ p.u., turbine initial speed $\omega_{\rm m0}=1.2$ p.u., initial output torque $T_{\rm m0}=0.83$ p.u.

APPENDIX D
PARAMETERS OF SAC, AGC, AND CONTROLLER PARAMETERS OF RSC AND GSC

$\varphi_0^+=2$, $\varphi_0^-=-2$, $\varepsilon_0^+=1.95$, $\varepsilon_0^-=1.95$, $u(0)=0$ rad, $K_\delta=0.4$, $K_{\rm f}=2$.

Speed regulator gains: $K_{\rm p}=3$, $K_{\rm i}=0.6$. Rotor-side converter current regulator gains: $K_{\rm p}=0.6$, $K_{\rm i}=8$. Grid-side converter current regulator gains: $K_{\rm p}=0.83$, $K_{\rm i}=5$. DC-bus voltage regulator gains: $K_{\rm p}=8$, $K_{\rm i}=400$. Pitch compensation gains: $K_{\rm p}=3$, $K_{\rm i}=30$.

APPENDIX E
PARAMETERS OF THE EXCITER AND PSS OF A SYNCHRONOUS GENERATOR

Fig. 15 presents the layout of a thyristor exciter with transient gain reduction, where $K_{\rm A}=400$, $T_{\rm R}=0.01$, $T_{\rm A}=1.2$, $T_{\rm B}=5.0$.

Fig. 16 presents the layout of a PSS of a synchronous generator, where $K_{\rm PSS}=25.0$, $T_{\rm s}=7.5$, $T_1=0.055$, $T_2=0.02$, $T_3=3.0$, $T_4=5.5$.

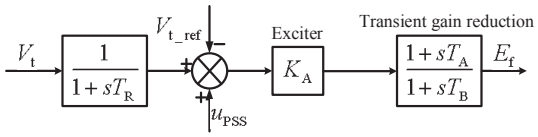

Fig. 15. The layout of the exciter of synchronous generators.

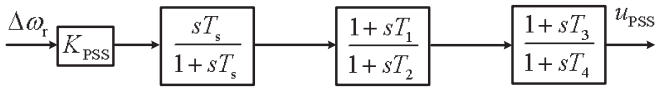

Fig. 16. The layout of the PSS of synchronous generators.

REFERENCES

[1] Y. Liu, Q. H. Wu, and X. X. Zhou, "Co-ordinated multiloop switching control of DFIG for resilience enhancement of wind power penetrated power systems," *IEEE Trans. Sustain. Energy*, vol. PP, no. 99, pp. 1–11, 2016.

[2] V. Gevorgian, Y. Zhang, and E. Ela, "Investigating the impacts of wind generation participation in interconnection frequency response," *IEEE Trans. Sustain. Energy*, vol. 6, no. 3, pp. 1004–1012, 2015.

[3] D. Zhang, Y. Wang, J. Hu, S. Ma, Q. He, and Q. Guo, "Impacts of PLL on the DFIG-based WTG's electromechanical response under transient conditions: analysis and modeling," *CSEE Journal of Power and Energy Systems*, vol. 2, no. 2, pp. 30–39, June 2016.

[4] N. R. Ullah, T. Thiringer, and D. Karlsson, "Temporary primary frequency control support by variable speed wind turbinesłpotential and applications," *IEEE Trans. Power Syst.*, vol. 23, no. 2, pp. 601–612, 2008.

[5] F. Díaz-González, M. Hau, A. Sumper, and O. Gomis-Bellmunt, "Participation of wind power plants in system frequency control: Review of grid code requirements and control methods," *Renew. Sust. Energy Rev.*, vol. 34, pp. 551–564, 2014.

[6] X. Yingcheng and T. Nengling, "Review of contribution to frequency control through variable speed wind turbine," *Renew. Energy*, vol. 36, no. 6, pp. 1671–1677, 2011.

[7] K. Vidyanandan and N. Senroy, "Primary frequency regulation by deloaded wind turbines using variable droop," *IEEE Trans. Power Syst.*, vol. 28, no. 2, pp. 837–846, 2013.

[8] A. Žertek, G. Verbič, and M. Pantoš, "A novel strategy for variable-speed wind turbines' participation in primary frequency control," *IEEE Trans. Sustain. Energy*, vol. 3, no. 4, pp. 791–799, 2012.

[9] L. Holdsworth, J. B. Ekanayake, and N. Jenkins, "Power system frequency response from fixed speed and doubly fed induction generator-based wind turbines," *Wind energy*, vol. 7, no. 1, pp. 21–35, 2004.

[10] P. Bousseau, R. Belhomme, E. Monnot, N. Laverdure, D. Boëda, D. Roye, and S. Bacha, "Contribution of wind farms to ancillary services," in *CIGRE General Meeting, Paris, France*, 2006.

[11] J. Morren, S. W. De Haan, W. L. Kling, and J. Ferreira, "Wind turbines emulating inertia and supporting primary frequency control," *IEEE Trans. Power Syst.*, vol. 21, no. 1, pp. 433–434, 2006.

[12] S. Wang, J. Hu, X. Yuan, and L. Sun, "On inertial dynamics of virtual-synchronous-controlled DFIG-based wind turbines," *IEEE Trans. Energy Convers.*, vol. 30, no. 4, pp. 1691–1702, 2015.

[13] S. Zhang, Y. Mishra, and M. Shahidehpour, "Fuzzy-logic based frequency controller for wind farms augmented with energy storage systems," *IEEE Trans. Power Syst.*, vol. 31, no. 2, pp. 1595–1603, March 2016.

[14] L. Miao, J. Wen, H. Xie, C. Yue, and W.-J. Lee, "Coordinated control strategy of wind turbine generator and energy storage equipment for frequency support," *IEEE Trans. Ind. Appl.*, vol. 51, no. 4, pp. 2732–2742, 2015.

[15] J. Morren, S. de Haan, W. Kling, and J. Ferreira, "Wind turbines emulating inertia and supporting primary frequency control," *IEEE Trans. Power Systems*, vol. 21, no. 1, pp. 433–434, Feb 2006.

[16] S. Li, R. Challoo, and M. J. Nemmers, "Comparative study of DFIG power control using stator-voltage and stator-flux oriented frames," in *Power & Energy Society General Meeting, 2009. PES'09. IEEE*. IEEE, 2009, pp. 1–8.

[17] P. Kundur, N. J. Balu, and M. G. Lauby, *Power system stability and control*. McGraw-hill New York, 1994, vol. 7.

[18] D. Liberzon and S. Trenn, "The bang-bang funnel controller for uncertain nonlinear systems with arbitrary relative degree," *IEEE Trans. Autom. Control*, vol. 58, no. 12, pp. 3126–3141, Dec 2013.

[19] Y. Liu, Q. H. Wu, and X. X. Zhou, "Coordinated switching controllers for transient stability of multi-machine power systems," *IEEE Trans. Power Syst.*, vol. PP, no. 99, pp. 1–13, 2015.

[20] Y. Liu, Q. H. Wu, H. T. Kang, and X. X. Zhou, "Switching power system stabilizer and its coordination for enhancement of multi-machine power system stability," *CSEE Journal of Power and Energy Systems*, vol. 2, no. 2, pp. 98–106, June 2016.

[21] Y. Han, M. Luo, X. Zhao, J. M. Guerrero, and L. Xu, "Comparative performance evaluation of orthogonal-signal-generators-based single-phase pll algorithmsła survey," *IEEE Trans. Power Electron.*, vol. 31, no. 5, pp. 3932–3944, 2016.

[22] "Characteristics and target values of the voltage supplied by the hydro-québec medium and low voltage systems," pp. 1–38, June 2001. [Online]. Available: http://www.hydroquebec.com/pdf/en/qualite_tension.pdf

[23] World Energy Council, "World energy resources: 2013 survey," pp. 1–468, 2013. [Online]. Available: http://www.worldenergy.org/publications/2013/world-energy-resources-2013-survey/

[24] Y. Liu, Q. H. Wu, X. X. Zhou, and L. Jiang, "Perturbation observer based multiloop control for the DFIG-WT in multimachine power system," *IEEE Trans. Power Syst.*, vol. 29, no. 6, pp. 2905–2915, Nov 2014.

Y. Liu was born in Inner Mongolia, he obtained a B.E. degree in Electrical Engineering from South China University of Technology (SCUT), Guangzhou, China, in 2012. He is currently pursing the Ph.D degree at the same area in SCUT. Now he is also with the Department of Electrical Engineering and Electronics, The University of Liverpool, as a honorary associate under the support of China Scholarship Council (CSC). His research interests include the areas of power system control and operation, smart grid and renewable energy.

L. Jiang (M'00) received the B.Sc. and M.Sc. degrees in electrical engineering from Huazhong University of Science and Technology (HUST), China, in 1992 and 1996, respectively; and the Ph.D. degree from the University of Liverpool, UK, in 2001. He is a Senior Lecturer in The University of Liverpool. His current research interests are control and analysis of power system, smart grid and renewable energy.

Q. H. Wu (M'91, SM'97, F'11) obtained a Ph.D. degree in Electrical Engineering from The Queen's University of Belfast (QUB), Belfast, U.K. in 1987. He worked as a Research Fellow and subsequently a Senior Research Fellow in QUB from 1987 to 1991. He joined the Department of Mathematical Sciences, Loughborough University, Loughborough, U.K. in 1991, as a Lecturer, subsequently he was appointed Senior Lecturer. In September, 1995, he joined The University of Liverpool, Liverpool, U.K. to take up his appointment to the Chair of Electrical Engineering in the Department of Electrical Engineering and Electronics. He is also with the School of Electric Power Engineering, South China University of Technology, Guangzhou, China, as a Distinguished Professor and the Director of Energy Research Institute of the University. Professor Wu has authored and coauthored more than 440 technical publications, including 220 journal papers, 20 book chapters and 3 research monographs published by Springer. He is a Fellow of IEEE, Fellow of IET, Chartered Engineer and Fellow of InstMC. His research interests include nonlinear adaptive control, mathematical morphology, evolutionary computation, power quality and power system control and operation.

X. X. Zhou (F'96) graduated from Tsinghua University in 1965. He is the Honorary President of China Electric Power Research Institute (CEPRI), academician of Chinese Academy of Science, and IEEE Fellow. He received an IEEE Nari Hingorani FACTS award in 2008. His main research interests include power system analysis and control, power system digital simulation, Flexible AC Transmission System (FACTS).